UNIVERSIDAD DE BARCELONA
Facultad de Física
Departamento de Electrónica
Laboratorio de Ingeniería y Materiales Electrónicos

ION BEAM SYNTHESIS OF SILICON-CARBON STRUCTURES AND RELATED MATERIALS

Memoria presentada por Lorenzo Calvo Barrio
para optar al grado de Doctor en Física

Director de Tesis: Dr. Alejandro Pérez Rodríguez

Programa de doctorado:
Micro i Optoelectrónica Física (bienio 92/94)

Barcelona, Mayo de 1999

3.3 SYNTHESIS OF SiC MICROSTRUCTURES

The possibility of defining SiC microstructures in Si technology gives interest for the improvement of the processes for synthesising higher quality SiC layers on Si substrates. Different kinds of micromachined devices, such as high temperature pressure sensors and capacitive accelerometers have been fabricated using as active layers β-SiC grown by CVD techniques on Si[14,15]. For these structures, the improvement in the structural quality of the SiC film formed by high dose ion implantation, in relation to that of the layers obtained by CVD techniques, which are characterised by a high density of defects related to the large mismatch between both lattices and to the Si cavities, would allow an improvement in the performance of the devices. In this context, it seems possible to develop microstructures with the ion beam synthesised layers, though this important issue needs to be proved.

This section deals with the fabrication of simple test microstructures such as thin membranes and self-standing structures with the ion beam synthesised layers. For this, a double etching process directly derived from Si technology has been designed. The high quality of the synthesised layers has allowed to obtain ultra-thin crystalline layers, with thickness as low as 120 nm and surface roughness in the range of 6-7 nm. This has required a previous study of the etch-stop properties of the implanted layers, which can also be applied as etch-stop layers in Si micromachining.

In this sense, one of the main problems related to micromachining technologies is the non-availability of suitable etch-stop layers. For complex structures with integrated electronics, buried layers with high enough values of etch selectivity and stable under high temperature processing are needed. Etch selectivity is defined as the ratio between the rate of the etched material and that of the etch-stop layer[16]. This value ranges from 1 (absence of any etch-stop effect) to infinite (ideal etch-stop behaviour), and in general selectivities in the range 10^2-10^3 are acceptable. For high precision microstructures, selectivities higher than 10^3 might be needed. Moreover, for an ideal interface between the etch layer and the etch-stop one, the roughness of the etched surface is determined by both the roughness of the initial surface and the selectivity of the layer. Therefore, layers with high enough selectivity present a significant decrease in the surface roughness. However, in general the interface between the etch layer and the etch-stop one is not ideal, and the roughness of this interface has also to be taken into account.

The main etch-stop techniques in Si technology are electrochemical etch-stop at a p-n junction and the use of heavily doped p^+ layers[16-19]. In the first case, the formation of contacts on the wafer is required in order to bias it, which is difficult to achieve on processed wafers. In the second case, etch-stop layers are obtained by doping with high B contents (typically higher than $6x10^{19}$ cm^{-3}). Highly B-doped Si shows very good etch selectivity in anisotropic etchants of Si, such as KOH, tetramethyl ammonium hydroxide (TMAH) or ethylene diamine pyrocatechol (EDP), and etch-rate selectivities as high as 5000 can be achieved[20,21]. However, this has two main problems, the strain induced by B in the lattice, which can lead to the generation of misfit dislocations in the structure, and B migration during the high temperature annealing. High temperatures can quickly redistribute B throughout the structure, reducing the B content below that needed for etch-stop behaviour and modifying the doping level of the surrounding areas. This constitutes a severe problem for the fabrication of integrated sensors, where the sensing element and the control electronics are made in the same wafer. Control electronics is usually based on complementary metal oxide semiconductor (CMOS) devices, and the fabrication of these devices requires high temperature processing, for example, in order to form wells. Unintentional doping modification, together with the loose of etch-stop behaviour, make CMOS processing impossible and most of the applications of the p^+ etch-stop are limited to micromechanical structures.

Ion implantation has several potential advantages for the fabrication of etch-stop layers, because of the possibility of obtaining buried layers in the Si wafer and its patternability. The depth of the buried layer and its thickness is controlled in a straightforward way by the implantation energy and dose. Buried layers at depths up to a few microns can be achieved by implanting at energies up to MeV. Moreover, complex patterns can be generated by implanting through masks or by using focused implantation beam equipments, which allow to obtain micrometrical spatial resolution.

Different authors[16,22-26] have reported the formation of layers with etch-stop behaviour by implanting different species (P, B, H, He, Ne, Ge, C, Si...) in Si at relatively small implantation doses (up to doses of order 10^{16} cm^{-2}). The etch-stop effect has been attributed mainly to implantation induced lattice damage, which reduces the carrier concentration in the implanted layer through the creation of deep level traps. These etch-stop layers are not stable under thermal annealing, even for anneal temperatures below 1000°C, due to the annealing induced damage recovery.

On the other hand, the layers obtained by ion implantation of C in Si at 500°C have the clear advantage in front of the others of the stability of the implanted specimen with the annealing treatment. The unavoidable drawback is the higher level of damage in the network as defects present in the Si substrate.

In the following section, the capabilities of the C implanted layers as etch-stop films in Si technology will be studied. The minimum C dose needed for this effect will be determined and special emphasis will be made in the achievement of an etch-stop layer stable under high temperature annealing (required for CMOS technology). The obtained data have been interpreted in terms of a percolation model in a binary SiC/Si system. Finally, the etch-stop behaviour of these layers is applied to the fabrication of simple microstructures, which will be described in the last section of this chapter.

3.3.1 ETCH-STOP BEHAVIOUR OF C IMPLANTED LAYERS

Etch-stop behaviour has been studied in the as-implanted and annealed samples described in section 3.1.1. As already indicated, these samples were obtained by implanting substoichiometric doses of C^+ in Si wafers at 500°C and an energy of 300 keV. The etch-stop analysis has been centred in samples implanted at doses of 10^{17} cm^{-2} and $5x10^{17}$ cm^{-2}.

Tetramethil ammonium hydroxide (TMAH) has been used as etchant solution, because of its higher compatibility with CMOS technology in comparison with other Si anisotropic etchants, such as KOH or EDP. Prior to the etching experiments, a 20 nm thick surface layer was removed by Reactive Ion Etching (RIE) in order to avoid that any residual surface contamination caused by the sample processing could alter the observation of the etch-stop behaviour of the buried layer. After this, part of the surface was covered with a 1 μm thick Pyrox SiO_2 film deposited at low temperature (400°C) and etching was performed in TMAH at 25% wt and 80°C during different times up to 1 hour. The etch-stop behaviour of the back interface between the implanted layer and the Si substrate has also been studied. For this, the surface of the top layer was thermally bonded to a silica wafer and the Si substrate was etched away.

With respect to the results, a sharp transition in the etch-stop behaviour has been observed between the samples implanted at doses of 10^{17} and $5x10^{17}$ cm^{-2}. For samples implanted at the lowest dose, no significant difference between the etch-rate of the buried layer and that of a Si reference layer was observed.

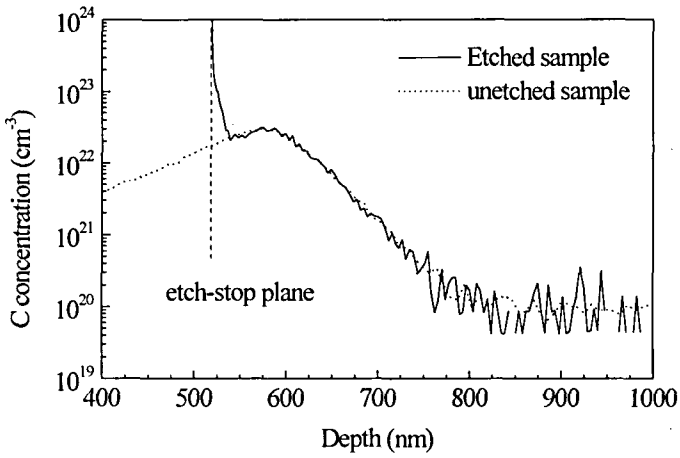

Figure 3.18 SIMS C profiles from the samples implanted at the highest dose, not etched and etched 1h in TMAH.

Conversely, for the highest implantation dose, the buried layer remains unetched in the TMAH solution after the maximum etching time of 1 hour. This has been observed for both the as-implanted and the annealed samples, what indicates the high thermal stability of the implanted layers. In both cases, a very smooth surface is obtained. The roughness of this surface has been measured by AFM, obtaining RMS values of 6-7 nm. These are similar to those obtained on the etched surface of samples implanted at highest doses, leading to stoichiometric SiC buried layers (in section 3.2).

The same behaviour has been observed for the lower interface. In this case, after an etching of the Si substrate, a membrane formed by the top Si layer and the remaining buried etch-stop one remained on the silica wafer. This behaviour was only observed for the samples implanted at the highest dose ($5x10^{17}$ cm^{-2}) as-implanted and annealed, and the morphology of the etched surface was found to be similar to that shown in figure 3.14.

In order to determine the minimum C concentration needed to achieve an efficient etch-stop behaviour, SIMS measurements have been performed on the etched samples. Figure 3.18 shows the SIMS C profiles from the as-implanted samples without etching and with 1 hour etching in TMAH.

For the etched sample, a surface peak is observed in the etch-stop plane. This peak is related to transitory effects in the SIMS measurements, and it is not taken into account. As shown in this figure, etching stops at a depth of about 60 nm above the implanted peak. Moreover, from this profile it is possible to estimate the ratio between the C concentration at the surface and that at the implanted peak. Since the peak concentration is proportional to the implanted dose, this allows to make a direct estimation of the threshold implantation dose for the formation of an etch-stop layer, being the estimated value in the range of $2\text{-}3\text{x}10^{17}$ cm^{-2} for the used implantation conditions (energy 300 keV, temperature 500°C). This is consistent with the disappearance of the etch-stop property at the lower implantation dose of 10^{17} cm^{-2}.

By correlating these SIMS profiles with the XPS measurements, the C content in the etch-stop plane in figure 3.18 can be determined. This is made assuming that the average density of the material in the buried layer depends linearly on the SiC to Si ratio, using those values from Si and β-SiC. For an implantation dose of $5\text{x}10^{17}$ cm^{-2}, a peak concentration of $3\text{x}10^{22}$ at/cm^3 is found, corresponding to the 63% of Si atoms in SiC phase as measured by XPS. This value was then used to calibrate the SIMS profile from the etched sample, which gives a surface concentration of about $1.7\text{x}10^{22}$ at/cm^3, corresponding to the implantation dose in the range $2\text{-}3\text{x}10^{17}$ cm^{-2}.

The sharp transition observed in the etch-stop behaviour of the samples implanted at the lowest and the highest dose has been interpreted in terms of a percolation mechanism, assuming the layer to be formed by a binary SiC/Si system and taking into account the inertness of SiC to the TMAH etchant. In this case, etching takes place as long as the etchant can flow through the Si regions in the layer. For a given threshold concentration of SiC grains, it becomes impossible for the etchant to find a path through the Si regions in the layer, and the etching stops.

This threshold has been estimated by means of a three-dimensional site percolation model[27]. In such a model, the SiC precipitates are represented by spheres of radius R, homogeneously placed at the nodes of a network with lattice parameter 2R and total length L >> R (R = 5-10 nm, according to TEM analysis). The probability for a node to be occupied by a sphere will be denoted by p, being p the fraction of cells that are occupied by a SiC sphere. The simplest approach in this model is to use a simple cubic network, and a more complex diamond network has also been considered. According to the type of network, the minimum value of the fraction p for which percolation occurs is p_c=0.3117 (cubic simple network) and p_c=0.428 (diamond network).

Taking into account the density of SiC, the threshold atomic concentration of C in the layer for etch-stop can be estimated from these values in a straightforward way, obtaining $0.8x10^{22}$ at/cm^3 (cubic network) and $1.08x10^{22}$ at/cm^3 (diamond network). This corresponds to threshold implantation doses of $1.33x10^{17}$ cm^{-2} for the simple cubic network, and $1.8x10^{17}$ cm^{-2} for the diamond one. These values are consistent with those estimated from the experimental data, in the range $2\text{-}3x10^{17}$ cm^{-2}, bearing in mind the simplicity of the used model.

The comparison of these data with those previously reported for etch-stop layers formed by N ion implantation[28] points out the higher efficiency of C in relation to N for etch-stop behaviour. In this last case, a threshold dose of $4x10^{17}$ N$^+$/cm^2 for implantation energy of 75 keV is needed to achieve an efficient etch-stop layer. This value is higher than that measured for the C implantation at 300 keV. In principle, decreasing the implantation energy would lead to an increase in the peak concentration and, hence, to a decrease in the threshold dose. In fact, according to TRIM, a threshold dose of $2.3x10^{17}$ cm^{-2} is expected for C implantation at 75 keV. Furthermore, it is worth remarking the high planarity of the etched surface that contrasts with the presence of pits in the etched surface from the N implanted ones.

The higher efficiency of C in relation to other implanted species, as Ge, Ar, Ne or Si has been previously reported by Feijoo et al[22] using EDP as an etchant, lower doses (of the order of $3x10^{16}$ cm^{-2}) and energies in the range of 35-200 keV. However, these authors observed a rapid degradation of the etch-stop efficiency with the annealing temperature, even at temperatures as low as 150°C. This contrasts with the very high stability of the layers produced by high dose implantation, in where SiC is synthesised. By increasing the implantation dose and (or) decreasing the energy, a continuous β-SiC layer can be achieved. The high crystalline quality and low residual strain level of the synthesised SiC would allow its use as precursor for the growing of high quality thicker SiC layers. Together with the etch-stop properties of the membranes, these excellent characteristics will motivate the fabrication of SiC microstructures on Si substrate.

3.3.2 FABRICATION OF MICROSTRUCTURES

The SiC microstructures have been fabricated according to the process schematically described in figure 3.19, which is directly derived from the standard Si bulk micromachining technology.

After a standard photolitography of positive resin, windows were defined by RIE through the buried layer down to a depth of 15 to 20 μm. Then, the samples were anisotropically etched in TMAH at the same conditions than those used for the etch-stop analysis. By this way, the Si was etched away from both above and below the buried layer. After a long enough etching time, the {111} planes of the Si substrate intersected below the implanted layer, due to their lower etch-rate and free standing membranes were obtained.

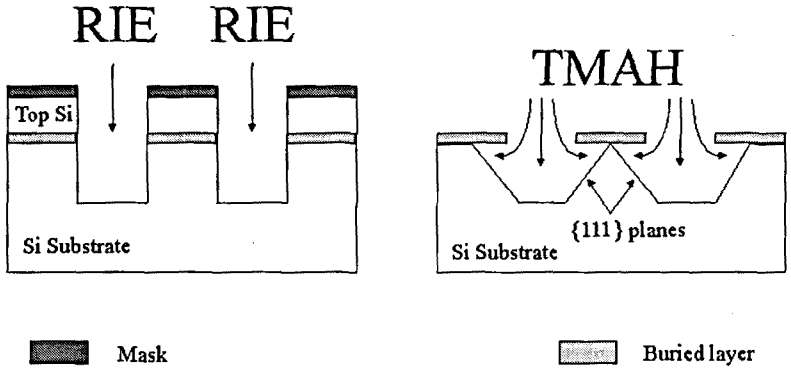

Figure 3.19 Scheme of the double etching process: (a) definition of windows through the structure by RIE, and (b) chemical anisotropic etching in TMAH.

Figure 3.20 shows cross-section SEM images of self standing membranes obtained from the sample implanted at a dose of $5x10^{17}$ cm^{-2} and an energy of 300 keV after 1 hour etching of the as-implanted (a) and 30 minutes etching of the annealed structures (b). The big pyramid observed below the membranes is formed by the intersection of the {111} planes from the Si substrate, which have a lower etch rate in TMAH etchant.

In the case of the as-implanted sample of figure 3.19, the membrane remains attached to the substrate by a small inverted pyramid, which does not appear in the case of the annealed samples. Moreover, in the annealed samples, the membranes are cut from the substrate after only 40 minutes of etching. This behaviour can be explained assuming the presence in the as-implanted sample of a layer with a slower etch rate below the buried layer, probably related to the implantation damage. This would correlate with the presence of {113} self-interstitial defects observed by TEM in this region.

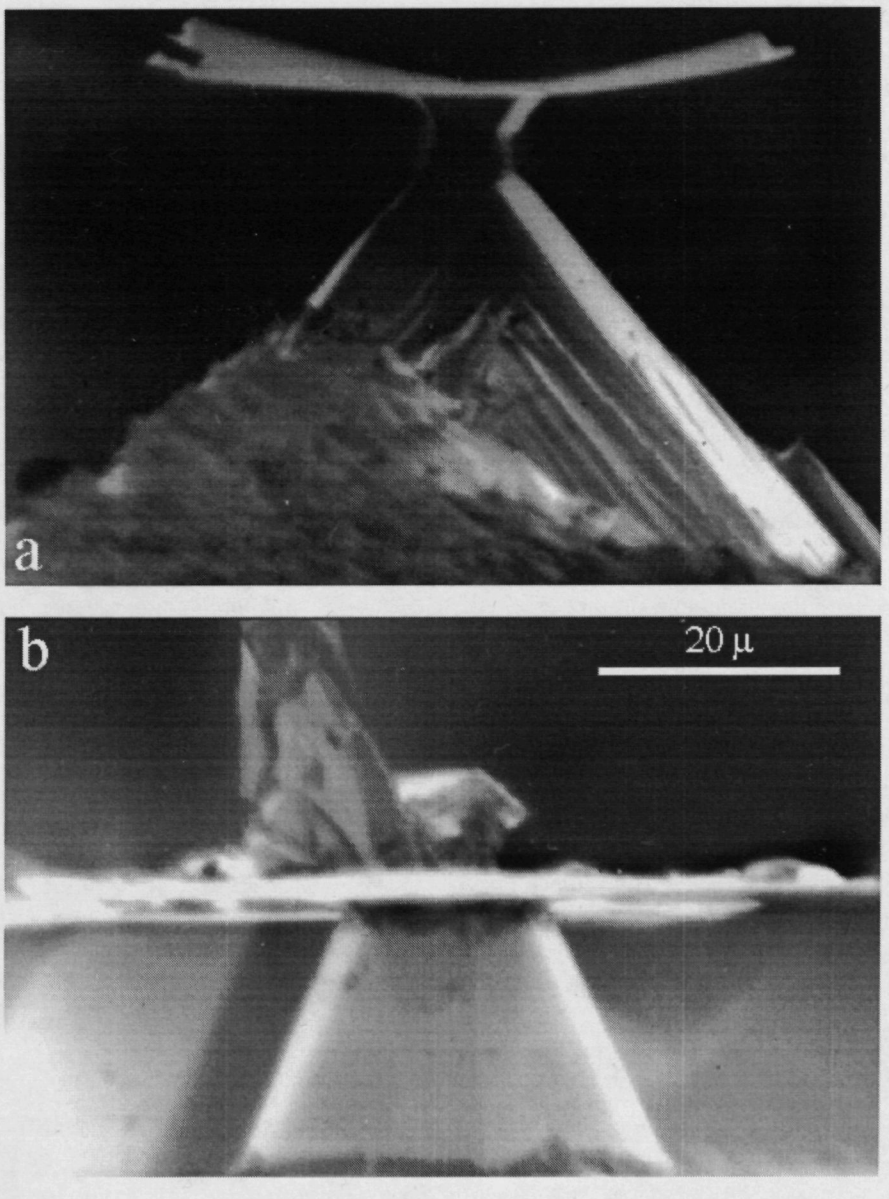

Figure 3.20 Cross-sectional SEM images of self-standing membranes from the sample implanted at the highest dose: (a) as-implanted 1h etched and (b) annealed 30' etched. The thickness of these membranes is of the order of 120 nm.

Similar anomalous etch stop effects obtained by self-implantation have already been reported for an EDP etchant[22]. These extended defects are removed by annealing the sample, which would account for the absence of such inverted pyramids in the annealed samples. In both cases, it is necessary to remark the extremely low value of the thickness of the membranes, which is of the order of 120 nm according to the SIMS profile shown in figure 3.18, together with the high surface planarity, with a RMS surface roughness in the range 6-7 nm.

On the other hand, the SEM images shown in figure 3.20 point out the existence of a significant stress gradient in the as-implanted samples. This is revealed by the curvature of the structures. This stress seems to be significantly released in the annealed samples. This behaviour agrees with the XRD data, which show a significant decrease of the residual strain in the SiC grains with the annealing, as indicated in section 3.1.3.

For stoichiometric thicker SiC layers than those described in section 3.2, the process described in figure 3.18 was modified due to the very low etch rate of SiC under RIE etching (about 20-30 nm/min for SiC under standard conditions, for which typical etch rate values in Si are about 15 μm/min). In this case, the use of an Aluminium mask (previously defined by a standard photolitography of positive photoresist) was necessary to stand the longer etching time needed.

Figure 3.21 shows the SEM image of different simple test structures, such as bridges and cantilevels fabricated in the annealed wafers. In this case, the high stiffness of SiC allowed the fabrication of beams as long as 100 μm and up to 40 μm wide in spite of their small thickness of 300 nm. The characterisation of these cantilevels by the micromechanical procedure developed by Serre et al[29] gives an average value of the Young modulus of the layer of 470 GPa. This is in excellent agreement with the usually accepted value of about 450 GPa in the literature for SiC[30,31]. Such a high value, more than twice higher than that of polysilicon (130 to 170 GPa depending on its fabrication process) is one of the key features that make SiC interesting for micromechanical applications.

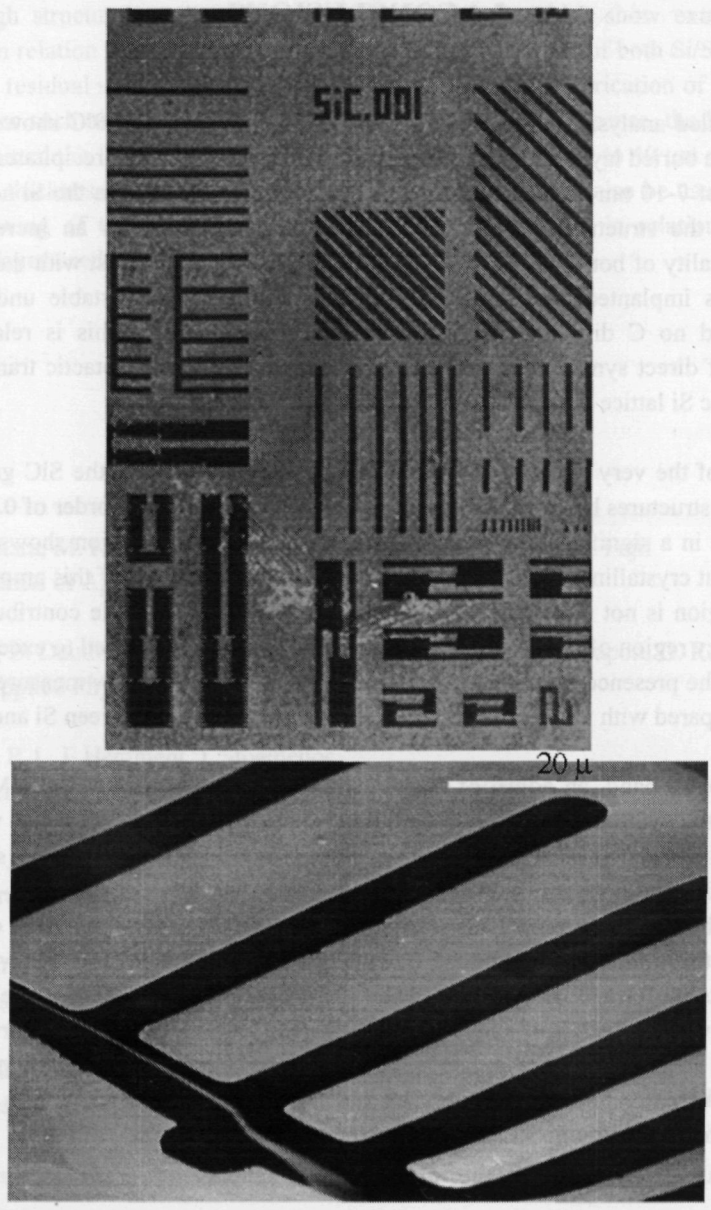

Figure 3.21 SEM image of a microstructure obtained from the sample implanted at the highest dose and annealed, after 30 minutes etching.

3.4 CONCLUSIONS

The detailed analysis of Si wafers implanted with C^+ ions at 500°C shows the direct formation of a buried layer with β-SiC crystalline precipitates. These precipitates have sizes in the range of 7-10 nm and have the same crystalline orientation than the Si network. An annealing of the structures at 1150°C during several hours allows an increase in the crystalline quality of both the Si and SiC crystalline phases. In contrast with the behaviour from samples implanted at RT, the C implanted profile is very stable under thermal annealing and no C diffusion towards the surface is observed. This is related to the dominance of direct synthesis of crystalline SiC, according to a topotactic transformation from the cubic Si lattice to the cubic β-SiC one.

In spite of the very high lattice mismatch between both lattices, the SiC grains in the as-implanted structures have residual strain of tensile character in the order of 0.1-1%. This strain relaxes in a significant way after annealing. HRTEM observation shows that a thin region without crystalline contrast surrounds SiC grains. The nature of this amorphous-like intergrain region is not clear, although the absence of any measurable contribution in the high frequency region of the Raman spectra suggests that it is not related to exceeding of C. In any case, the presence of this envelope allows to understand the low measured values of strain as compared with those expected from the lattice mismatch between Si and SiC.

On the other hand, an adjust of the implantation parameters by the TRIM simulator code allows the synthesis of a buried continuous stoichiometric β-SiC layer, with abrupt interfaces with the top Si and substrate regions. These layers have been successfully applied for the synthesis of simple micromechanical test devices. For this, a previous analysis of the etch-stop properties of the C implanted Si layers has been carried out, determining the minimum amount of C content needed for etch-stop behaviour. SIMS measurements performed on samples etched in TMAH (25% wt, 80°C) have allowed to estimate this value, which is of about $1.7x10^{22}$ ions/cm^2 and corresponds to a threshold dose for etch-stop behaviour in the range $2\text{-}3x10^{17}$ cm^{-2} for the used implantation conditions (energy 300 keV, temperature 500°C). This has been interpreted in terms of a percolation model, assuming a binary Si/SiC structure of the buried layer.

The high structural quality of the synthesised layers, which show extreme etching selectivity in relation to the Si lattice, together with the abruptness of both Si/SiC interfaces and the low residual strain after the annealing have allowed the fabrication of self-standing test structures such as membranes, bridges and cantilevels. In this sense, the high stiffness of SiC permitted the fabrication of beams as long as 100 μm and up to 40 μm wide, in spite of their low thickness (of about 300 nm). The implanted layer can also be used as the seed for the growing of thicker SiC films, with potential advantages in relation to the thin carbonised layer used in the CVD growing of SiC in Si.

3.5 REFERENCES

1. A. Chayahara, M. Kiuchi, A. Kinomura, Y. Mokuno, Y. Horino, K. Fujii
Japanese Journal of Applied Physics *32* p. 1286 (1993)

2. P. Martin, B. Daudin, M. Dupuy, A. Ermolieff, M. Olivier, A. M. Papon, G. Rolland
Journal of Applied Physics *67* p. 2908 (1990)

3. A. Nejim, P. L. F.Hemment, J. Stoemenos
The Electrochemical Society Proceedings *94-11* p. 167 (1994)

4. L. Simon, J. Feruré, A. Mesli, J. J. Grob, J. L. Balladore
Nuclear Instruments and Methods in Physics Research B *112* p. 330 (1996)

5. A. De Veirman
Ph. D. Thesis, University of Antwerpen (1990)

6. J. K. N. Lindner, A. Frohnwieser, B. Rauschenbach, B. Stritzker
Materials Research Society Symposium Proceedings *354* p. 171 (1995)

7. J.K.N.Lindner, K.Volz, U.Preckwinkel, B.Götz, A.Frohnwieser, B.Rauschenbach, B.Stritzker
Materials of Chemistry and Physics *46* p.147 (1996)

8. U.Preckwinkel, J.K.N.Lindner, B.Stritzker, B.Rauschenbach
Nuclear Instruments and Methods in Physics Research B *120* p. 125 (1996)

9. C. J. Mogab
Journal of the Electrochemical Society *120* p. 932 (1973)

10. S. Isomae, T. Ishiba, T. Ando, M. Tamura
Journal of Applied Physics *74* p. 3815 (1993)

11. A. De Veirman, J. VanLanduyt, W.Skorupa
Philosophical Magazine A *64* p. 513 (1991)

12. A. Bachrouri
M. D. Thesis, University of Barcelona (1998)

13. L.Calvo-Barrio, A.Pérez-Rodríguez, A.Romano-Rodríguez, J.R.Morante, J.Montserrat
Materials Science and Technology *11* p. 1187 (1995)

14. G. Krötz, W. Legner, Ch. Wagner, H. Möller, H. Sonntag, G .Müller
Digest of Technical Papers of Eurosensors IX *2* p. 186 (1995)

15. G. Krötz, Ch. Wagner, W. Legner, H. Sonntag, H. Möller, G. Müller,
Institute of Physics Conference Series *142* p. 829 (1996)

16. S. D. Collins
Journal of the Electrochemical Society *144-6* p. 2242 (1997)

17. H. A. Waggener
Bell Systems Technology Journal *49* p. 473 (1970)

18. H. Seidel, L. Csepregi, A. Heuberger, H. Baumgartel
Journal of the Electrochemical Society *137* p. 3626 (1990)

19. N. F. Raley, Y. Sugiyama, T. Van Duzer
Journal of the Electrochemical Society *131* p. 161 (1984)

20. Ch. E. Hunt, G. V. Rouse, C. Harendt, M. C. Green
IEEE Proceedings SOS/SOI Technical Conference p. 145 (1990)

21. D. Feijóo, J. C. Bean, L. J. Peticolas, L. C. Feldman, W. C. Liang
Journal of Electronic Materials *23* p. 493 (1994)

22. D. Feijoo, V. Lehman, K. Mitani, U. M. Gösele
Journal of the Electrochemical Society *139* p. 2309 (1992)

23. K. C. Lee
Journal of the Electrochemical Society *137* p. 2556 (1990)

24. K. C. Lee, J. Silcox, C. A. Lee
Journal of Applied Physics *54* p. 4035 (1983)

25. A. C. Ipri
U.S. Patent 4,092,209 (1978)

26. D. J. Day, G. W. R. Middelton, T. W. Janes, J. C. White, V. J. Mifsud
Journal of the Electrochemical Society *131* p. 407 (1984)

27. *Introduction to percolation theory*, Ed. D.Stauffer
Taylor & Francis, London-Philadelphia (1985)

28. A. Söderbärg
Journal of the Electrochemical Society *139* p. 561 (1992)

29. C. Serre, P. Gorostiza, A. Perez-Rodriguez, F. Sanz, J. R. Morante
Sensors and Actuators A *67/1-3* p. 215 (1998)

30. L. G. Matus, L. Tang, M. Mehregany, D. J. Larkin, P. G. Neudeck
Institute of Physics Conference Series *137* p. 185 (1993)

31. *Silicon Carbide*, Eds. R. C. Marshall, J. W. Faust Jr., C. E. Ryan
Publications of University of Carolina, Columbia (1974)

CHAPTER 4

CARBON IMPLANTATION INTO SiGe ALLOYS AND RELATED STRUCTURES

This chapter is devoted to the study of the C implantation processes in SiGe layers. The first aim of these experiments is to deepen in the knowledge of the mechanisms of SiC ion beam synthesis in these layers, in order to determine the influence of parameters such as the chemical composition, the strain level and the bond length of the target material. In addition, SiGeC complex systems have a strong interest due to the possibility of incorporating substitutional C into Si and SiGe lattices without loosing crystalline quality. This allows working with band-gap and strain engineering in Si based technologies, something mainly restricted to III-V compounds up to now. In this context, the possible modification of the synthesised phase has also to be investigated in terms of the formation of this ternary system.

The organisation of this chapter is as follows. In the first section the application of optical and structural techniques such as XRD, Raman scattering and FTIR, for the strain and chemical composition analysis of group IV Si-Ge-C based alloys is reviewed. This is very important for the study of the implanted structures, as some controversy has arisen in literature on the validity of these techniques to quantify the incorporation of C into substitutional positions in the lattice. This section is based on the detailed analysis of a reference matrix of $Si_{1-x-y}Ge_xC_y$ pseudomorphic layers which were grown in the University of California (Davis) by Chemical Vapour Deposition techniques[1].

The remaining sections are organised in a similar way than in the previous chapters. First of all, the study of the implantation and recrystallisation of amorphous layers is presented. This involves the use of RT medium to high dose C implantations. Afterwards, the processes involved when the implantations are performed in crystalline substrates and avoiding the amorphisation of the samples are analysed. According to the previous study on Si implanted wafers, this can be achieved by heating the samples at 500°C during implantation. Finally, the main conclusions of this chapter are summarised in last section.

4.1 STRAIN AND CHEMICAL SPECTROSCOPIC ANALYSIS OF Si-Ge-C BASED CRYSTALS

One of the most used techniques in the analysis of epitaxial films and heterostructures is XRD. The reason of that is its high sensitivity for measuring strain in the crystalline layers. Strain values in the range of 10^{-5}-10^{-6} are routinely measured, and values as low as 10^{-8} can also be detected[2,3]. The analysis of epitaxial layers by XRD is usually performed by measuring rocking curves. These curves are obtained by fixing the diffracted angle of the X-ray beam and rotating the sample around a certain orientation, which corresponds to a well-known crystalline direction of the substrate. By combining spectra measured with different orientations of the sample, the lattice constants of the film parallel and perpendicular to the plane of the interface of the epitaxial layer with the substrate can be determined with a high accuracy. According to the expressions from section 1.1.2, both the strain value in the layer and the lattice constant of the corresponding strain free alloy can be obtained from a straightforward application of elasticity theory.

The measurement of the strain free lattice constant allows to determine the composition of the layer, assuming the validity of Vegard's law[4]. This law predicts that the lattice parameter of a crystalline alloy is given by the linear interpolation of the lattice constants from the parent semiconductors. For $Si_{1-x}Ge_x$ binary alloys, some deviation of this simple law has been observed[5], mainly for x values of about 0.5. In this case, the experimental data have been fitted with the following expression (all the different lattice parameters are in angstroms[6]).

$$a_{SiGe} = x \cdot a_{Ge} + (1-x) \cdot a_{Si} - 0.00436 \cdot x^3 + 0.03265 \cdot x^2 - 0.02829 \cdot x$$

In principle, this can also be applied to determine the amount of substitutional C in $Si_{1-y}C_y$ and $Si_{1-x-y}Ge_xC_y$ alloys. However, the validity of Vegard's law in these systems is still under discussion in literature. Theoretical calculations that deviate considerably from this law[7] have been reported. To clarify this point, detailed XRD measurements have been performed in a matrix of $Si_{1-x-y}Ge_xC_y$ pseudomorphic layers grown by the Rapid Thermal Chemical Vapour Deposition technique (RTCVD), being the nominal x composition range between 0 and 0.46, and y between 0 and 4%. These samples were grown in the University of California (Davis) and in the Lawrence Semiconductor Research Laboratory Inc (Temple, AZ), and were designed as reference samples for detailed XRD and Raman scattering measurements. The correlation of these data with RBS and SIMS composition analysis corroborates the validity of Vegard's law in the determination of the C content in substitutional sites in the layer[1]. The best agreement has been achieved by assuming a value of Poisson coefficient of 1/3.

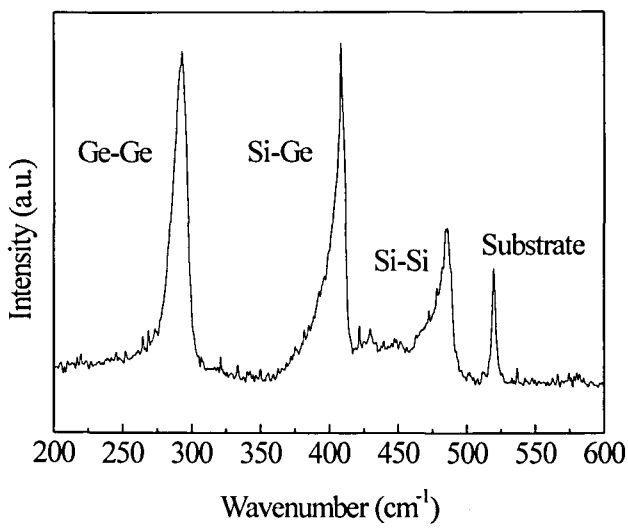

Figure 4.1 First order Raman spectrum from a $Si_{1-x-y}Ge_xC_y$ strained layer on Si substrate.

On the other hand, Raman scattering offers an interesting alternative to XRD for the strain and the chemical composition analysis of these systems. For $Si_{1-x-y}Ge_xC_y$ alloys, the first order Raman spectrum shows three main lines, related to the Si-Si (around 500 cm^{-1}), Si-Ge (around 400 cm^{-1}) and Ge-Ge (around 300 cm^{-1}) vibrational modes. This can be seen in figure 4.1, which shows the first order Raman spectrum from a $Si_{1-x-y}Ge_xC_y$ strained layer.

These modes show a linear dependence on both the average strain, and the chemical composition, which is related to the mass disorder and the microscopic strain effects,

$$\omega_{Si-Si}(cm^{-1}) = 520 - 68 \cdot x + (190 \pm 40) \cdot y_{sub} - 830 \cdot \eta$$

$$\omega_{Si-Ge}(cm^{-1}) = 400.5 + 14.2 \cdot x + (320 \pm 43) \cdot y_{sub} - 575 \cdot \eta$$

$$\omega_{Ge-Ge}(cm^{-1}) = 282.5 - 16 \cdot x + (370 \pm 125) \cdot y_{sub} - 384 \cdot \eta$$

where x is the Ge content in the lattice, η is the strain in the plane of the interface with the substrate, and y_{sub} is the atomic concentration of substitutional C. These expressions were first proposed by Melendez-Lira et al[8], and its validity was later experimentally corroborated[1]. Hence, the measurement of the spectral shift of the three main modes allows to determine from a single spectrum both the Ge and the substitutional C contents as well as the strain value in the lattice.

The quantification of the amount of C in substitutional possitions in a $Si_{1-y}C_y$ lattice can also be done from the measurement of the intensity of the Local Vibrational Mode (LVM) of substitutional C in Si, at about 605 cm^{-1}. This mode is Raman and infrared active, and hence can be detected in both Raman and IR spectra. For IR, there is a well-established standard, which relates the integral intensity of the LVM peak with the substitutional C content for systems in equilibrium, where C concentration is below its solubility limit[9] ($3.5x10^{17}$ cm^{-3}). More recently, Meléndez-Lira et al have reported the validity of this calibration for C contents much higher than the solubility limit[10]. These authors have measured $Si_{1-y}C_y$ layers made by ion implantation and laser annealing with effective atomic C ratios up to 0.5%. From the same samples, they have also observed a clear correlation between the integral intensity of the LVM mode in the Raman spectra and the C content. The following relationship for the quantification of substitutional C is proposed, with I_{LVM} and I_{Si} the integral intensities of the LVM mode and the first order Raman Si peak, respectively.

$$\frac{I_{LVM}}{I_{Si}} = (3.7 \pm 0.2) \cdot y_{sub}$$

However, it is necessary to bear in mind that the validity of these IR and Raman calibrations in Si-Ge-C ternary alloys is not completely clear.

4.2 CARBON IMPLANTATION INTO AMORPHOUS SiGe LAYERS

$Si_{1-x}Ge_x$ amorphous layers with thickness from 70 to 80 nm were grown on (100) Si substrates by magnetron RF sputtering. Two targets of Si and Ge were used, and the selected Ge content in the layers was of 14%. Deposition conditions were RT, Ar^+ pressure at $5x10^{-3}$ mbar, a Si target continuous power at 200 W and a Ge target pulsed power with maximum of 200 W and minimum of 30 W (30% cycles). Deposition time was 30 minutes.

Two series of samples, called A and B, have been synthesised. In A series, in order to pre-amorphise the Si substrate region down to a depth of about 235 nm before the C implantation, the SiGe/Si structures were implanted with Si^+ ions at RT, with an energy of 170 keV and a dose of $2x10^{15}$ cm^{-2}. For B series, the SiGe amorphous layers on the Si crystalline substrates were directly implanted with C ions. The C implanted energy, 25 keV, was selected to obtain the C peak in the interface region between the SiGe amorphous layer and the Si crystalline substrate, in order to compare the incorporation of the C atoms in both Si and SiGe lattices after thermal recrystallisation. The intermixing of the original SiGe/Si interface was also planned to enhance the possible solid phase epitaxial re-growth from the Si substrate. Figure 4.2 shows the C implanted profile simulated by TRIM in the SiGe/Si structure with the implant energy of 25 keV, showing the C implanted peak position close to the SiGe/Si interface.

During implantation, the samples were kept at RT. Samples were implanted at three different doses, $5x15^{15}$ cm^{-2}, $6x10^{16}$ cm^{-2} and $2x10^{17}$ cm^{-2}. According to TRIM, these correspond to C implanted peak contents of 1.4%, 15% and 37%. The lowest dose was selected to achieve a Ge to C content ratio in the implanted peak close to the strain compensation in the Si-Ge-C ternary alloy. From Vegard's law, the strain compensation is predicted for a Ge to C content ratio of 8.3:1, and different authors[11-14] have reported strain compensated pseudomorphic films grown by different techniques with ratios in the range 8 to 12. This peak C content of 1.4% is close to the metastable solubility limit, which has been reported by Strane et al for C incorporation into the Si lattice by ion implantation and SPE processes[15]. Above this value, local bond deformation between the Si and C atoms in the amorphous/crystalline interface is postulated for the formation of such defects as microtwins and stacking faults along <111> planes, which limit C supersaturation in the Si lattice. The other doses correspond to C peak contents much higher than those achieved for metastable alloys[8], which are up to about 3%, and the formation of SiC is expected. Pieces from all the samples have been annealed at 700°C and 900°C during 1 hour in a N_2 ambient.

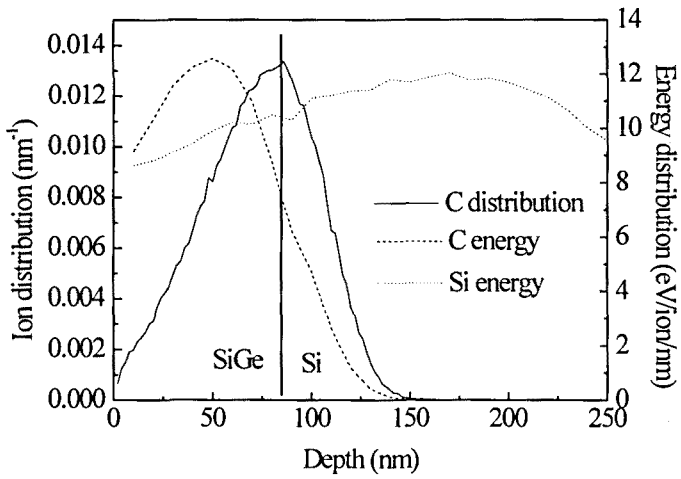

Figure 4.2 C implanted profile simulated by TRIM in A series of SiGe/Si structure with C energy of 25 keV and Si energy of 170 keV.

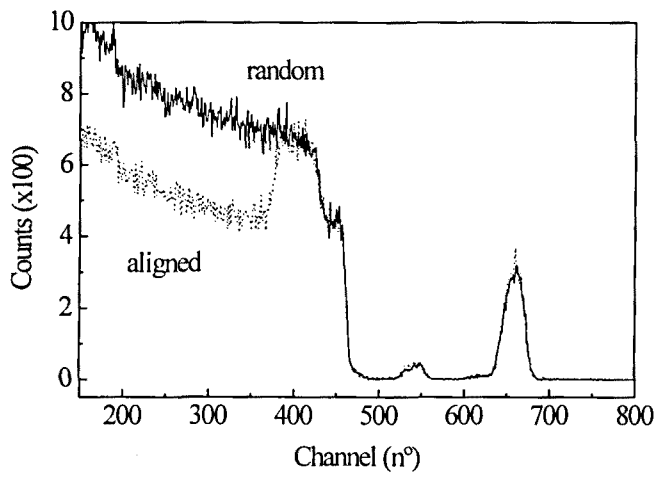

Figure 4.3 RBS random and aligned spectra from A series C implanted at $2x10^{17}$ cm^{-2}.

4.2.1 STRUCTURAL ANALYSIS OF AMORPHISATION AND RECRYSTALLISATION

The thickness of the ion beam amorphised Si region and its behaviour under thermal annealing has been determined from Rutherford backscattering (RBS) channelling measurements. RBS spectra were measured in the facilities available at the FZR (Dresden, Germany), using He^+ ions accelerated at 1.5 MeV. Figure 4.3 shows the RBS random and aligned spectra from a sample of A series (preamorphised) that was implanted with a C dose of $2x10^{17}$ cm^{-2} ions. Ions scattered by Si atoms give a RBS continuous signal from channel 464. This maximum energy corresponds to the scattering with Si surface atoms. The yield measured at lower channels is given by the amount of the Si atoms at the corresponding depth. The dip observed in the surface region is related to the lower content of Si in the SiGe film, obviously due to the existence of Ge atoms. In this sense, scattering of Ge atoms, which are heavier than Si ones, gives a peak at the higher channel 670. In a similar way, C atoms have a superimposed signal to the continuum Si spectrum from the substrate around channel 175, but the amount of C is not enough to have risen the peak. Moreover, the small peak centred on channel 550 is an artefact product of some resonance in the analyser. Finally, due to the existence of a correlation between channels and depth, a detailed study of the RBS spectrum allows to determine the different thickness of the layers. In this case, a SiGe film thickness of 70-80 nm can be corroborated from the FWHM of the peak centred at 670.

Figure 4.3 also shows the spectrum obtained when the incident beam is aligned in a low-density crystalline direction of the substrate. Channelling of incident ions in low-density paths causes a decrease in the scattered yield. Such defects as impurities or host atoms in intertitials positions will produce an increase in the aligned yield. So the comparison between both random and aligned spectra gives information of the crystalline quality of the layer and allows to quantify the residual damage. Thus, the amorphisation of the layer (loss of long range order, 100% of damage) is obtained when both spectra are equal. This is the case for all A series (pre-amorphised samples) whose spectra show an amorphous layer up to 310 nm in depth, due to the existence of a 245 nm thick amorphous Si film below the SiGe one.

On the other hand, for B series (not pre-amorphised samples), the RBS measurements performed on the as-implanted samples show an increase in the thickness of the surface amorphous layer with the C implanted dose. The thickness values, estimated from the channelling spectra, are of 84 nm (dose $5x10^{15}$ cm^{-2}), 135 nm (dose $6x10^{16}$ cm^{-2}) and 158 nm (dose $2x10^{17}$ cm^{-2}), respectively. This is due to the amorphisation of the Si region below the SiGe layer by the C^+ implantation.

Figure 4.4 shows a schematic diagram of the SiGe amorphous layer and the Si regions amorphised by C^+ implanted ions in B series, and C^+ plus Si^+ implanted ions in the case of A series. The different regions are labelled as I, II and III.

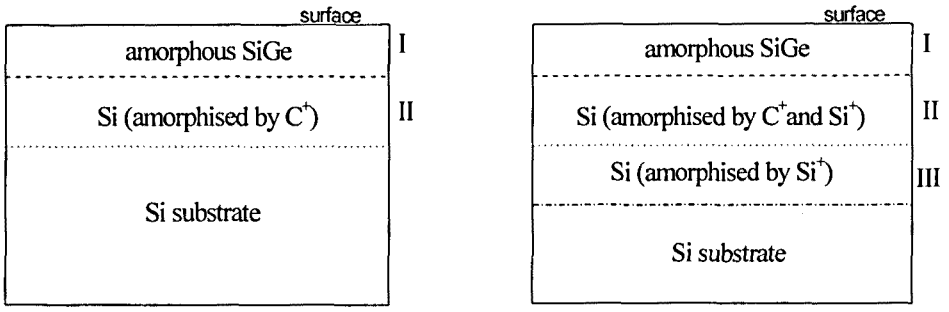

Figure 4.4 Schematic diagram of SiGe amorphous layer and Si regions amorphised by C^+ in B series at left, and C^+ plus Si^+ in A series, at rigth.

Annealing at 700°C allows SPE recrystallisation of the amorphous Si region below the C implanted layer (region III). According to this, the thickness of the remaining amorphous layer is similar in both series and it depends only on the C implanted dose. Only for the samples implanted at the lowest dose, fully epitaxial recrystallisation of Si takes place. For these samples, RBS channelling spectra show an amorphous-like surface layer that corresponds to the SiGe one. The similar yield between the channelled and random spectra in this layer is due to the polycrystalline recrystallisation of the SiGe layer, as corroborated by Raman scattering and TEM analysis. For the highest doses ($6x10^{16}$ cm^{-2} and $2x10^{17}$ cm^{-2}) the remaining amorphous layer corresponds to that amorphised by the C^+ implanted ions (region II in figure 4.4). This indicates that epitaxial crystallisation is inhibited by the high C content in these samples, which agrees with the behaviour already observed for C^+ ion implanted Si wafers (described in chapter 2). For these samples, epitaxial recrystallisation in the structure of regions II and III is only observed after annealing at 900°C.

These results agree with the behaviour observed from the Raman spectra. Figure 4.5 shows the Raman spectra measured from all samples of A series (Si preamorphised). These spectra were measured at the same conditions than in the previous chapters (backscattering configuration using a Raman microprobe with an objective magnification x100, excitation wavelength 457.9 nm). In principle, the spectra measured on B series are very similar to these.

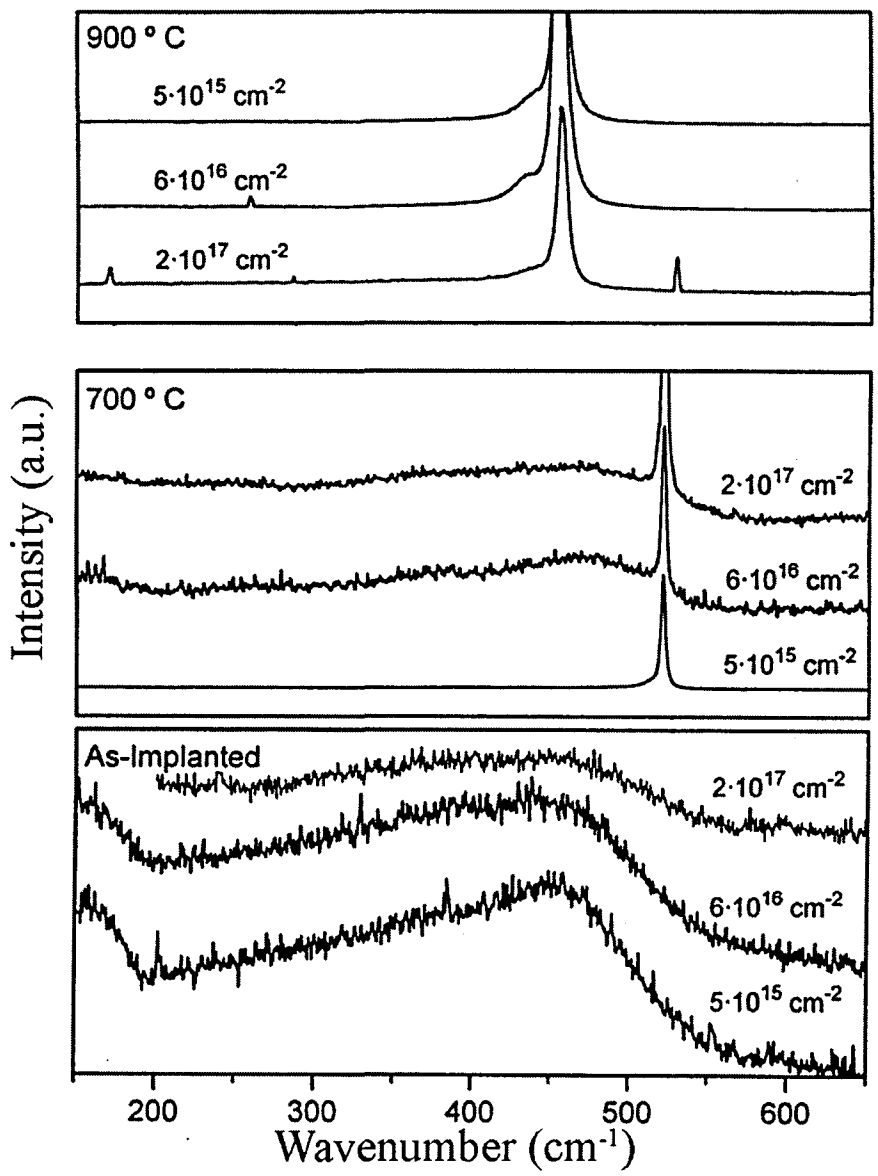

Figure 4.5 Raman spectra measured from all A series.

Spectra from as-implanted samples are basically broad bands characteristic from amorphous materials. Samples implanted at the lowest C dose show a main band centred in about 470 cm^{-1}. This band corresponds to the TO mode of amorphous Si. In contrast, highest C dose implies a modification in band's shape, due to the presence of C in the amorphous layer[16].

On the other hand, spectra from samples annealed at 700°C show the disappearance of amorphous bands only in the lowest C implanted samples. In this case, a first order Raman peak from Si crystalline is observed at 520 cm^{-1} together with a lower frequency contribution. By fitting these spectra with two lorentzian functions, both peaks are assigned to the Si substrate and the $Si_{1-x}Ge_x$ recrystallised layer, respectively. As the corresponding RBS spectrum shows an 'amorphous' $Si_{1-x}Ge_x$ layer equal in thickness to the not treated one, it is possible to conclude that, recrystallisation of the layer has been completed in a polycrystalline way by annealing at 700°C.

In samples implanted at highest C doses, it is necessary an annealing at 900°C for the disappearance of the amorphous bands. Spectra from these samples only present the Si peak from the substrate and the contribution of the $Si_{1-x}Ge_x$ polycrystalline layer.

As indicated, spectra from B series (not preamorphised, and not shown in the figure) are similar to those explained. Nevertheless, differences between both series are observed in relation to the intensity of the Si crystalline peak from the substrate. Table IV-I shows the intensity (in arbitrary units) of this peak for samples annealed at 700°C. The results for the lowest C implanted sample are worth noticing. In this sample, Si substrate contribution is definitively higher in the sample previously amorphised with Si^+ implantation (A series). This behaviour is related to the presence of a high density of structural defects originating at the depth corresponding to the position of the amorphous/crystalline interface before annealing. These defects are characteristic of the SPE process, and are known as EOR (End of Range) defects. These defects have been extensively reported in the literature[17-19].

For the sample implanted at the lowest C dose without preamorphisation, the amorphous/crystalline interface is located at about 10 nm from the SiGe/Si interface. This implies the appearance of a high density of defects in the surface region of the Si substrate from the annealed samples, which produce a decrease in the intensity of the Si Raman peak. For the samples previously amorphised with the Si^+ implantation, EOR defects appear at a higher depth, being the amorphous/crystalline interface at a depth of about 310 nm from the sample surface. This determines a significant decrease in the contribution of this damaged region in the Raman spectra, bearing in mind the strong absorption of light in the samples.

C DOSE (cm^{-2})	A SERIES INTENSITY (A.U.) (Si preamorphised)	B SERIES INTENSITY (A.U.)
$5X10^{15}$	117	84
$6X10^{16}$	4.9	5.4
$2X10^{17}$	9.9	9.5

Table IV-I Raman intensity (in arbitrary units) of the Si substate peak (520 cm^{-1}) for all samples annealed at 700°C, with and without Si preamorphisation.

By fitting with two lorentzian curves the main Si mode and the shoulder at lower wavenumbers it is possible to determine the shift of the Si-Si mode from the SiGe layer in relation to the Si susbtrate for the recrystallised samples. However, the low intensity of this mode gives a very high uncertainty in the measurement of this shift, of the order of 0.5 cm^{-1}. The samples implanted at the lowest dose and annealed at 700°C show a shift of the mode in the range between –9 and -10 cm^{-1}, and is similar to that observed in reference SiGe layers which were not implanted before the annealing. According to the expressions from section 4.1, a shift of -9.5 cm^{-1} is expected for a fully relaxed (strain free) $Si_{0.86}Ge_{0.14}$ layer. This strongly suggests that C is not incorporated in the SiGe lattice. For the samples implanted at the highest doses, shifts of about -7.5 cm^{-1} for dose $6x10^{16}$ cm^{-2} and in the range between –9 and -9.5 cm^{-1} for dose $2x10^{17}$ cm^{-2} are measured. In this case, the situation is more complex, as there are changes in the Ge content in the layers (as will be shown in the next section), and residual damage and strain can also significantly affect the position of the Raman modes.

4.2.2 CHEMICAL-PHYSICAL ANALYSIS

Figure 4.6 shows the FTIR transmission (normal incidence) spectra measured from the different as-implanted and annealed A series samples. In principle, these spectra are similar to those measured from B series samples. Some first features from these spectra can be noticed. First of all, it is clear the presence of the LVM C mode at 607 cm^{-1} in the spectra from the samples implanted at the lowest dose. The intensity of this mode is higher for the sample annealed at 700°C. This, together with the Raman data already discussed, indicates that for this dose C is effectively incorporated in substitutional sites in the Si substrate region which recrystallises epitaxially. An increase in the annealing temperature up to 900°C leads to a decrease in the intensity of the LVM mode, fact that indicates a lower degree of incorporation of C in substitutional positions. In these samples, there is not a detectable signal related to the Si-C absorption band.

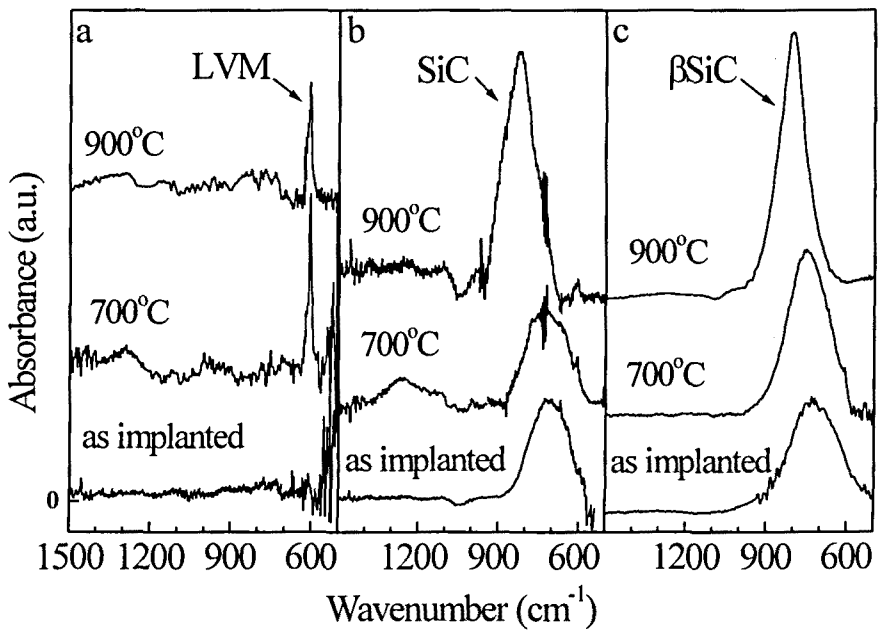

Figure 4.6 FTIR absorbance spectra from the as-implanted and annealed A series implanted at different doses (a) $5x10^{15}$ cm^{-2}, (b) $6x10^{16}$ cm^{-2} and (c) dose $2x10^{17}$ cm^{-2}.

As indicated in the section 4.1, for this implanted dose it is possible to correlate the area of the LVM peak with the incorporation of C in substitutional sites. The data obtained for the 700°C annealed sample, the one with the highest LVM peak, show that in the more favourable case a 39% of the implanted C is placed in these sites.

Moreover, for samples implanted at the intermediate dose the spectra are characterised by the Si-C absorption band (in the region of 700-900 cm^{-1}). Samples as-implanted and annealed at 700°C show a similar broad gaussian shaped band, which is characteristic of amorphous SiC. An annealing at 700°C leads also to a small contribution of the LVM C mode. This indicates that, in this case, C is partially incorporated in the Si lattice. However, the intensity of this mode is much lower than that from the sample implanted at the lowest dose and annealed at 700°C, which means a much lower susbtitutional C content. The majority of C implanted atoms are bonded to Si, forming an amorphous SiC phase. It is necessary to remark that Raman scattering measurements performed in the 1000-1500 cm^{-1} spectral region do not show any contribution from C-C modes. This is related to the value of the implanted dose, which gives a C content far below that from stoichiometric SiC (according to TRIM, the C peak atomic content at this dose is of about 15%). As already discussed in chapter 2, for substoichiometric amorphous SiC almost all C atoms are bonded to Si, being the probability of formation of C-C bonds very low.

Annealing this sample at 900°C leads to an increase in the intensity and a decrease in the FWHM of the SiC absorption band, which is related to the recrystallisation of the sample. However, this band is still gaussian in shape. It is centred at 804 cm^{-1} and has a FWHM of 140 cm^{-1}. This indicates the presence of a strongly distorted SiC crystalline phase. Besides, the intensity of the LVM mode decreases.

Therefore, the samples implanted at the highest dose do not show any contribution from the LVM C mode. The only feature of the spectra is the C absorption band, which has a gaussian amorphous-like shape for both samples as-implanted and annealed at 700°C. In this case, Raman scattering measurements also show the absence of a significant contribution from C-C bonds, which agrees with a C content below the stoichiometry. Annealing at 900°C leads, in this case, to a strong improvement in the crystalline quality of SiC. Only for the sample implanted at the highest dose and annealed at the highest temperature the spectrum becomes lortentzian in shape, being centred at 804 cm^{-1} and with a FWHM of 120 cm^{-1}. This clearly implies the formation of the β-SiC phase.

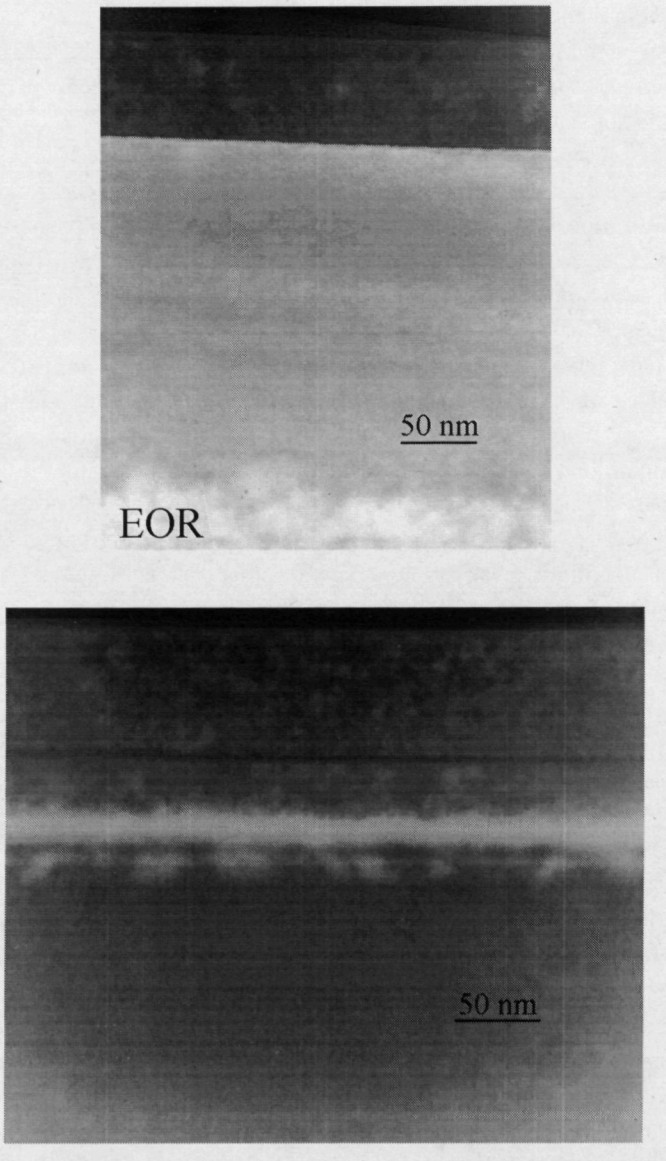

Figure 4.7 Cross-section TEM images from an A series sample implanted at $5x10^{15}$ cm^{-2} and annealed at 700°C (top) and a B series sample implanted at $6x10^{16}$ cm^{-2} and annealed at 900°C (bottom).

These data have also been corroborated by the TEM analysis of the processed samples. The main results obtained from TEM are summarised in figure 4.7. This figure shows the cross-section images for (a) a sample of the A series implanted at the lowest dose and annealed at 700°C and (b) a sample of the B series implanted at the intermediate dose and annealed at 900°C. The cross-section image at top shows the presence of EOR defects at a depth of about 300 nm, which extend deeper into the substrate. This correlates with the position of the crystalline/amorphous interface that, for all the A series samples, is located at a depth of about 310 nm. This image also shows the polycrystalline nature of the top SiGe layer. Moreover, at the original SiGe/Si interface a line of bright contrast can be observed. This probably corresponds to a native oxide layer in the wafer surface before the SiGe deposition. In principle, the surface of the wafers was cleaned using a standard procedure before their processing. However, this did not avoid the formation of a very thin oxide at the surface just before charging the wafers in the sputtering chamber. The presence of this interface layer could explain the interruption of the epitaxial regrowth from the Si substrate in the top SiGe layer. In this sense, the C implantation was not able to destroy this interface, in spite of the fact that the projected range of the C ions was close to this interface.

The aspect of the corresponding B series sample (not shown) is very similar. A relevant difference is that although in this sample EOR defects also appear, they are just below the SiGe/Si interface and their size is much smaller. This corroborates the hypothesis that the C implantation did amorphise the upper part of the Si substrate, in agreement with the RBS data. The improvement of the substrate crystallinity near the SiGe/Si interface in the A series is in agreement with the Raman spectra, which show a higher intensity of the Si line from the substrate region for the A series samples implanted at the lowest dose.

In figure 4.7 (bottom), a B series sample implanted at the intermediate dose and annealed at 900°C is shown. The structure is quite similar to that from the sample implanted at the lowest dose. The bright line, as already indicated, would correspond to the oxide native layer. However, in this case, a second polycrystalline layer has been formed below this interface, which seems to be a continuation of the top one. In this sample, it has not been possible to find any diffraction feature corresponding to crystalline SiC. This agrees with the FTIR data, which show the contribution from Si-C bonds in probably a strongly distorted crystalline phase.

As already indicated, for the highest implantation dose randomly oriented β-SiC crystalline grains are formed after the annealing at 900°C. This can be seen in the electron diffraction pattern of figure 4.8, which shows the presence of additional diffraction rings, corresponding to the (111) planes of β-SiC.

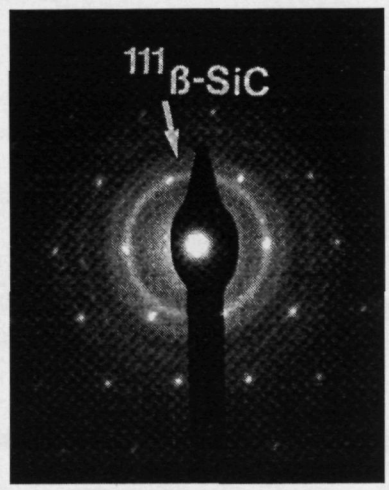

Figure 4.8 TED pattern from a B series sample implanted at $2x10^{17}$ cm^{-2} and annealed at 900°C.

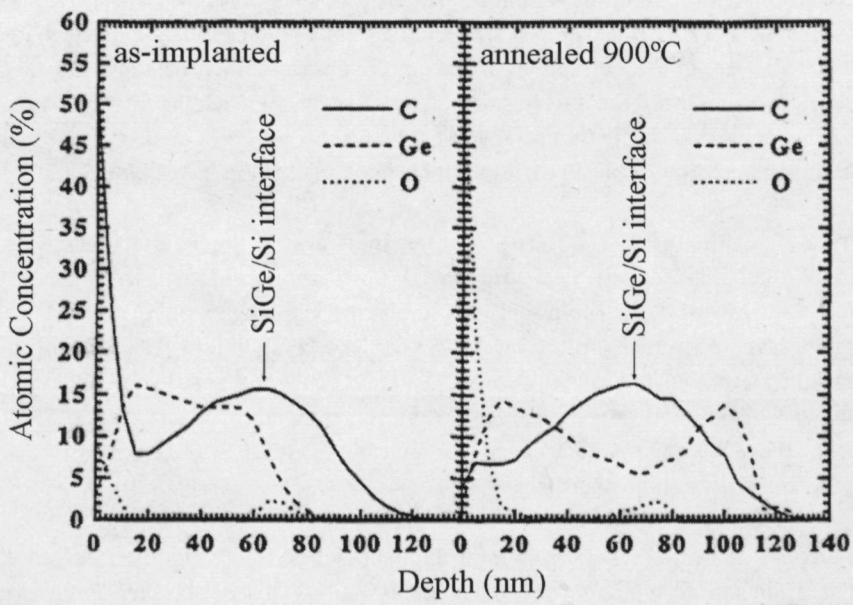

Figure 4.9 C, Ge and O AES depth profiles from the B series implanted at $2x10^{17}$ cm^{-2}.

The similar behaviour of the A and B series samples despite the very different levels of damage in the substrate region suggests that SiC crystallisation in the cubic polytype is enhanced by the highest C content in the samples.

The chemical analysis of the processed samples has been completed with AES measurements. The depth distribution of the different species has been analysed on samples sputtered with Ar^+ atoms. Figure 4.9 shows the C, Ge and O profiles from the samples implanted at the highest dose, as-implanted and annealed at 900°C. Again, samples from the A and B series show the same behaviour. First of all, the O profile is located in the SiGe/Si interface region (between 60 and 80 nm), which corroborates the high stability of the native oxide layer (SiO_2) after the sputtering deposition of the SiGe layer, the ion implantation and the annealing. However, the most striking feature from this figure is the existence of a Ge migration from the C implanted region towards the Si substrate. This contrasts with the high stability of the C implanted profile, which does not show significant changes with the annealing. The stability of the C profile is probably related to the formation of an amorphous SiC phase in the as-implanted state of the sample. The annealing at 900°C leads to the formation of crystalline β-SiC grains randomly oriented in the Si lattice matrix.

On the other hand, Ge has the following difussivity value in the Si lattice, lower than that from the C in Si,

$$D^{Ge} = 6 \times 10^5 \cdot e^{(-5.3eV/KT)} cm^2 / s$$

As a result, the diffusion length, L, is of about 2 nm. This short value contrasts with the strong Ge migration observed in the figure. A similar behaviour has already been observed by Warren et al[20] in $Si/Si_{1-x-y}Ge_xC_y/Si$ structures produced by RTCVD (Rapid Thermal CVD) and treated by RTA (Rapid Thermal Annealing) processes at temperatures in the range from 1000°C to 1300°C. In this work, and in contrast with the Ge behaviour, which difusses with the annealing treatments towards regions below and above the Si, SIMS measurements did not reveal any changes in the C distribution. C remains in the buried layer precipitating like β-SiC.

In the present case, Ge diffusion is probably enhanced by the formation of the SiC crystaline grains, while SiC precipitates are being formed. Ge segregates and moves towards regions with lower Ge concentration. This leads to the formation of a complex SiGe/SiC/SiGe heterostructure.

4.2.3 INCORPORATION OF CARBON IN SUBSTITUTIONAL SITES VERSUS SYNTHESIS OF SiC

The results obtained in these samples can be summarised attending to the dose value as follows. Firstly, at the lowest implanted dose ($5.5x10^{15}$ cm^{-2}) SiC precipitates are not observed, even after annealing at 900°C. However, LVM modes in the FTIR spectra from the annealed samples are clearly seen, what indicates the C incorporation in substitutional sites in the Si lattice. A maximum C incorporation of 39% of the implanted dose is done in the 700°C annealed sample. When increasing the annealing temperature from 700°C to 900°C, the percentage of C slowly decreases.

At the intermediate implanted dose ($6.6x10^{16}$ cm^{-2}), and previously to the annealing, FTIR spectra show the absorption band due to the Si-C bond in an amorphous material. After annealing at 700°C, the LVM mode appears with a much lower intensity than in the lowest implanted dose, together with the absorption band of the Si-C amorphous bond. An annealing at 900°C makes the intensity of the LVM mode to decrease, showing an intense absorption peak close to the position corresponding to the β-SiC. The gaussian peak shape, together with its width, suggests the existence of highly distorted β-SiC grains. On the other hand, it has been not possible to obtain any signal associated with the β-SiC crystalline in TED images. This could be due to the low crystalline quality of these grains.

At the highest implanted dose ($2x10^{17}$ cm^{-2}), the LVM mode is absent in the FTIR spectra. As-implanted and 700°C annealed samples show an absorption band from Si-C amorphous material. The sample annealed at 900°C presents an intense lorentzian peak, corresponding to the absorption of a crystalline SiC in β phase. TED images corroborate this point, showing supplementary rings identified with this phase. The presence of rings and the absence of spots indicate the random orientation of crystals.

All these data imply that both C incorporation in substitutional sites in the network and the formation of SiC crystals are strongly determined by the C concentration presented in the samples. For concentrations lower than 1-2%, C is preferably located in substitutional sites in the network and no SiC formation is observed, even after annealing at 900°C. However, a decrease in the C substitutional incorporated to the network is detected at this temperature of annealing, which is in accordance with Strane et al data[21]. For higher concentrations, up to 15%, coexistence between C in susbtitutional places and the highly distorted SiC crystalline is obtained. An increase in the C concentration in the implanted region up to a maximum of the order of 37% drives forward a drastic improvement of the crystallinity in the SiC grains, together with the absence of any C substitutional signal.

The correlation of these data with those about microstructure suggests that the incorporation of substitutional C is related to the SPE recrystallisation of the Si substrate. This agrees with the observation that the epitaxial crystallisation is broken when SiC nanocrystals are formed.

On the other hand, all the samples in which annealing processes have promoted the formation of SiC crystals, already presented a Si-C amorphous absorption band in the FTIR spectra before the annealing. The existence of Si-C bonds in the amorphous matrix strongly promotes the formation of SiC nanocrystals with the annealing. This is similar to the previous observations in C implanted Si wafers, and it is related to the high stability of the Si-C bonds.

Moreover, the improvement in the crystalline quality for the samples implanted at the highest dose suggests that the growth of SiC precipitates is distorted for concentration of medium range (up to 10%). This behaviour is not clear and could be related to the formation of C aggregates and Si interstitials, as a step between the incorporation of C substitutional to the Si network and the growth of SiC grains. Strane et al indicate the formation of aggregates rich in C as a previous step to the SiC precipitation, from the study of thermal stability of $Si_{1-y}C_y$ strained heterostructures obtained by ion implantation of C and SPE[21].

Finally, the analysis of the Raman spectra indicates that the C incorporation takes place in a preferred way in the Si substrate, which recrystallises epitaxially. This behaviour could be related to the higher local bond distortion expected around a substitutional C atom in the SiGe lattice than in the Si one, due to the higher bond length of the relaxed SiGe crystal. A strong local distortion around the substitutional sites is reported to be the key mechanism that limits the C incorporation in the lattice an the epitaxial recrystallisaton of the implanted layers[21].

4.3 CARBON IMPLANTATION INTO SiGe EPITAXIAL LAYERS

This section deals with the study of medium to high dose C ion implantations in SiGe epitaxial layers. In this case, and in contrast to the previous sections, the crystallinity of the implanted layers is preserved by implanting the wafers at 500°C. As already indicated, the main motivation of these experiments is to analyse the influence of the chemical composition and the strain in the target crystal on the ion beam synthesised phases. An additional interest is to complete the study performed on the amorphous systems, in order to clarify the role played by Ge and its behaviour under ion implantation and annealing processes. An important point is to analyse the possible presence of Ge enhanced by the diffusion processes that have been observed in the amorphous layers when recrystallisation occurs.

4.3.1 SAMPLES AND PROCESSES

Epitaxial $Si_{1-x}Ge_x$ layers with different composition and strain values have been implanted at 500°C. Two very different layers have been chosen so as to analyse the possible effects of both parameters, the Ge content and the strain, in the synthesised phases,

i) fully strained (pseudomorphic) $Si_{0.73}Ge_{0.27}$ layer (SL) with thickness of 73 nm, and
ii) Ge rich fully relaxed $Si_{0.45}Ge_{0.55}$ layer (RL) with thickness of 180 nm.

These layers were grown by MBE techniques and, in both cases, a highly phosphorous doped Si buffer layer was used. The presence of this buffer layer in the structures has not allowed the FTIR analysis of the samples.

In figure 4.10, the two TEM images from each type of samples corroborate the crystalline quality of the $Si_{1-x}Ge_x$ starting material. For the SL layer, no defects are observed in the cross-section TEM image, which is related to its pseudomorphic nature. This contrasts with the RL layer, where relaxation of SiGe leads to the formation of a high density of MISFIT dislocations. Relaxation of the layer occurs because its thickness is beyond the critical value for pseudomorphic growth[22]. However, in this case dislocations are efficiently confined in the interface region between the SiGe layer and the Si substrate, and no dislocation is observed to propagate towards the surface. A remarkable feature in this sample is the extremely flat surface in spite of the high Ge content and the state of relaxation.

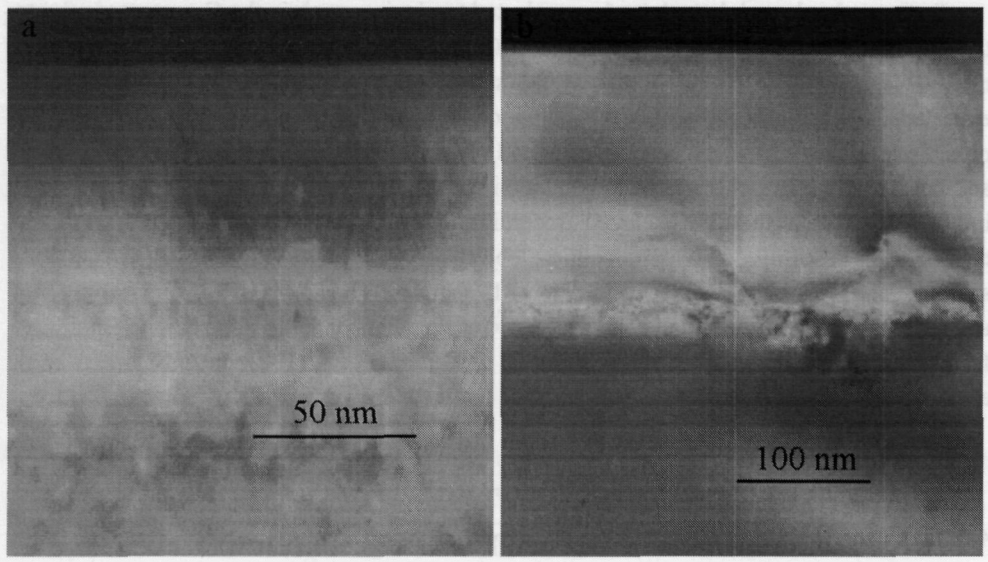

Figure 4.10 TEM images from SL (left) and RL (right) samples before any treatment.

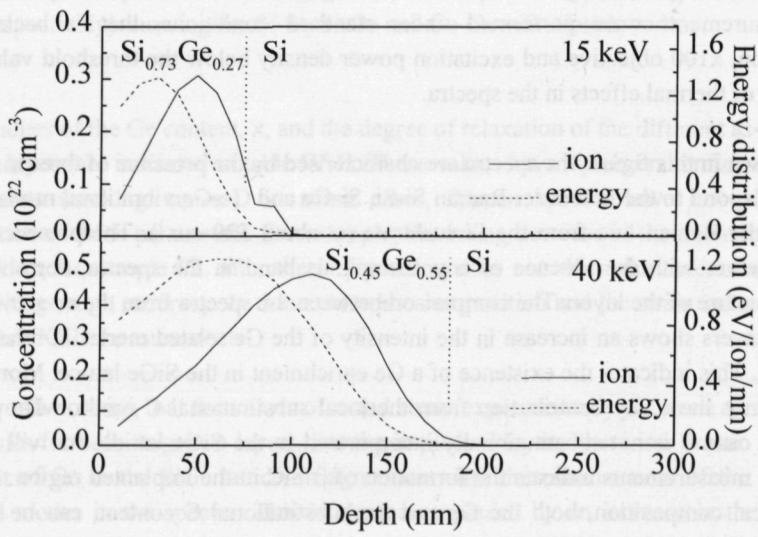

Figure 4.11 TRIM simulation from C implantation in SL (top) and RL (bottom) samples.

Different implanted doses have been selected to obtain a peak in the C content similar to the Ge one. In both cases, this corresponds to C content values well above those obtained in metastable binary and ternary alloys so the subsequent formation of SiC phases is to be expected. This was chosen because the main motivation of this experiment is to determine the possible influence of the ion beam synthesised phases on the target lattice parameters, strain and composition. The energies of implantation have been selected to keep almost all the C implanted profile in the $Si_{1-x}Ge_x$ layer. According to the TRIM simulation (figure 4.11), the energies and doses needed to achieve these objectives were 15 keV and $6x10^{16}$ cm^{-2} for SL samples, and 40 keV and $2x10^{17}$ cm^{-2} for RL samples. The implanted samples were not annealed to avoid any thermally induced SiC precipitation or lattice relaxation. Finally, to facilitate the comparison between SiGe and Si implanted layers, (100) virgin Si wafers were also implanted at the same conditions.

4.3.2 ION BEAM SYNTHESIS OF β-SiC IN SiGe

The strain and composition in the as-grown and implanted layers have been investigated by Raman scattering and XRD measurements. Figure 4.12 shows the Raman spectra measured in the different samples, using an excitation wavelength of 457.9 nm. As in the previous cases, these measurements were performed under standard conditions, that is backscattering configuration, x100 objective and excitation power density below the threshold value for the appearance of thermal effects in the spectra.

As shown in this figure, the spectra are characterised by the presence of three main peaks, which correspond to the first order Raman Si-Si, Si-Ge and Ge-Ge vibrational modes, besides the first order Raman line from the Si susbtrate (at about 520 cm^{-1}). The presence of these modes, together with the absence of any amorphous band in the spectra, corroborates the crystalline nature of the layers.The comparison between the spectra from the as-grown and the implanted layers shows an increase in the intensity of the Ge related modes in relation to the Si-Si mode. This indicates the existence of a Ge enrichment in the SiGe lattice. Moreover, the spectra do not show any contribution from the local substitutional C mode, what points out that in this case C is not substitutionally incorporated in the SiGe lattice. As will be shown later, XRD measurements indicate the formation of β-SiC in the implanted region. The strain and chemical composition, both the Ge and the substitutional C content, can be quantified from the position of the different main peaks in figure 4.12, according to the empirical relationships given in section 4.1. The analysis of the Raman spectra with these expressions allows to corroborate the absence of C incorporation in the SiGe lattice.

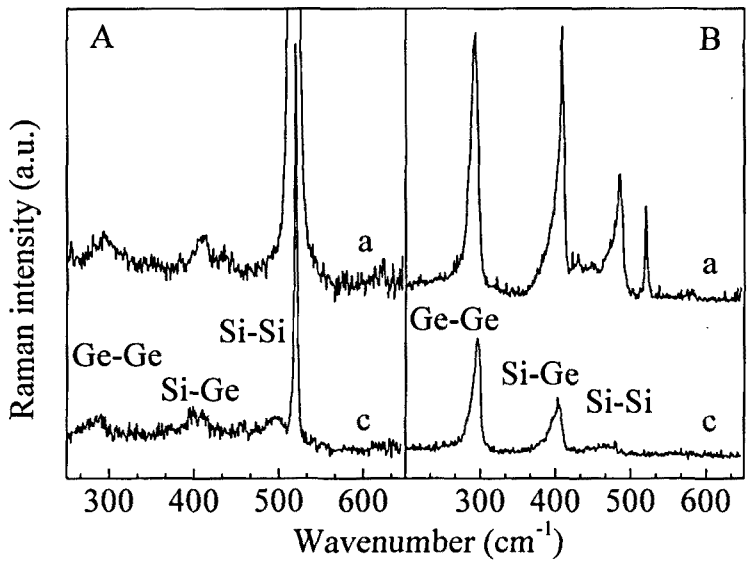

Figure 4.12 Raman spectra for the as grown (a) and implanted (b) SiGe layers (A and B, RL and SL, respectively) showing the Si-Si, Si-Ge and Ge-Ge vibrational modes.

The values of the Ge content, x, and the degree of relaxation of the different as-grown and implanted layers are indicated in table IV-II. These values have also been confirmed by XRD measurements (rocking curves). In some cases, Raman spectra have not allowed the quantification of these parameters. For example, the strong decrease in the intensity of the Si-Si mode from the sample RL after the implantation does not allow the determination of its position with enough accuracy. In these cases, the composition and the strain values had to be derived from XRD measurements.

It is worth noticing that the values of x and strain experimentally obtained agree with the nominal ones for both as-grown layers. For the implanted layers, there is a drastic increase in the content of Ge in the SiGe lattice, in agreement with the enhancement of the Ge related vibrational modes in the spectra. This is also accompanied by an increase in the degree of relaxation of the layers, which is especially conspicuous for the SL sample. In this case, the implantation causes a strong relaxation of about 75% in the previous fully strained SiGe lattice.

Sample	X	Degree of relaxation
SL as grown	0.27	0%
SL implanted	0.42	75%
RL as grown	0.56	84%
RL implanted	0.77	88%

Table IV-II Values of x and strain relaxation for the SiGe lattice in the different samples obtained from both the Raman and XRD spectra.

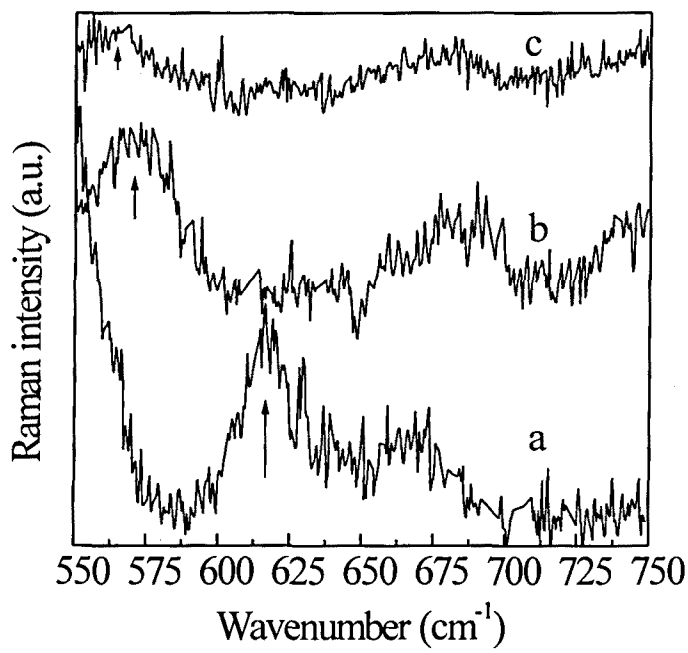

Figure 4.13 Raman spectra in the 550-750 cm^{-1} region for samples bulk Si (a), RL as grown (b) and RL implanted (c).

Figure 4.13 shows the Raman spectra measured in the RL as-grown and implanted layers in the 550-750 cm^{-1} region, together with the spectrum from bulk Si. As already indicated, the spectra from the implanted layers do not show any contribution from the C LVM, fact that corroborates that C is not efficiently incorporated in the substitutional sites.

On the other hand, the spectra from the RL layers are characterised by the presence of a peak centred at about 563 cm^{-1} and 556 cm^{-1} in the as-grown and implanted samples respectively. The shape of this peak, after a baseline correction, is similar to that of the second order Si line at 610 cm^{-1}. According to this, this peak could be attributed to the second order Si line from the relaxed SiGe lattice, which would be shifted towards lower wavenumbers due to the high Ge content. This agrees with the higher shift towards lower wavenumbers of the peak from the implanted samples which, according to the data from table IV-II, show an increase in the Ge content in the SiGe lattice. For the SL samples, the low thickness of the SiGe layer has not allowed to determine this mode with enough accuracy.

The spectra measured on the different samples in the 1000-2000 cm^{-1} region do not show any significant contribution from C-C vibrational modes. This, together with the XRD and TEM analysis of the samples that will be shown in the following, suggests that C is mainly in the form of β-SiC precipitates. As indicated previously, the absence of SiC modes from the Raman spectra is due to the lower optical absorption and Raman efficiency of SiC in relation to Si or SiGe. On the other hand, the XRD spectra from the implanted samples show the presence of peaks from β-SiC. This corroborates the direct synthesis of β-SiC in SiGe by C implantation.

Sample	$Strain_{200}$	$Strain_{111}$	FWHM
SL implanted	1.2%	1.2%	4.6°
Si implanted (SL)	2.1%	1.5%	5.8°
RL implanted	1.3%	2.4%	7.2°
Si implanted (SL)	1.3%	1.4%	4.8°

Table IV-III Values of strain in SiC crystals measured from the shift of the (200) and (111) XRD peaks, together with the FWHM of the (200) peak from the w-scans.

Moreover, the SiC grains are crystalline oriented in relation to the implanted lattice, the relationships being $[001]_{SiC}||[001]_{Si}$ and $(110)_{SiC}||(110)_{Si}$, in a similar way to that observed in Si. Table IV-III shows values of strain in SiC crystals obtained from the shift of the (200) and (111) XRD peaks, together with the FWHM of the (200) peak from the w-scans. The values of these parameters measured in equivalent Si implanted samples have also been included.

As it is shown, strain in the SiC crystals depends on the implanted matrix. The SiC grains formed in the relaxed implanted layer show higher strain than those formed in the corresponding Si sample. This is probably related to the higher bond length of the relaxed SiGe crystal in relation to Si. The topotactic transformation implies a conversion of the SiGe lattice into a SiC one, forming the implanted C atom bonds with the Si atoms in the lattice. The residual tensile stress in the SiC crystals is related to an injection of interstitials from the implanted layer, which in this case are mainly Ge atoms, as will be shown later. This explains the drastic Ge enrichment observed in the SiGe matrix. Thus, an increase in the bond length of the target matrix leads to an increase in the tensile strain of the SiC grains, due to the higher free volume generated from the interstitial flux in the implanted region. This is also accompanied by a higher crystalline distortion of the grains, which gives rise to a higher degree of missorientation in the SiC crystals, as shown by the increase of the FHWM of the (200) peak from the w-scan. The presence of a high density of extended defects in the form of dislocations in the region close to the substrate in the as-grown relaxed layer also contributes to a higher missorientation of the crystals formed below the projected range.

On the other hand, the strain values in the SiC crystals formed in the SiGe strained matrix are lower than those in the grains formed in the corresponding Si sample. In this case, the compressive strain in the SiGe matrix partially compensates the residual tensile strain in the grains. The lower crystalline distortion of the grains would result in an improvement of their crystalline orientation. This agrees with the decrease in the FWHM of the (200) peak in relation to the corresponding Si sample, as shown in the table.

4.3.3 CHEMICAL-PHYSICAL IN-DEPTH ANALYSIS OF EPITAXIAL SiGe IMPLANTED LAYERS

The in-depth analysis of the implanted samples has been performed by XPS measurements on Ar^+ sputtered samples. This has been completed with the TEM cross-section inspection of the layers. Figure 4.14 shows the Ge and C composition profiles from the as-grown and implanted samples.

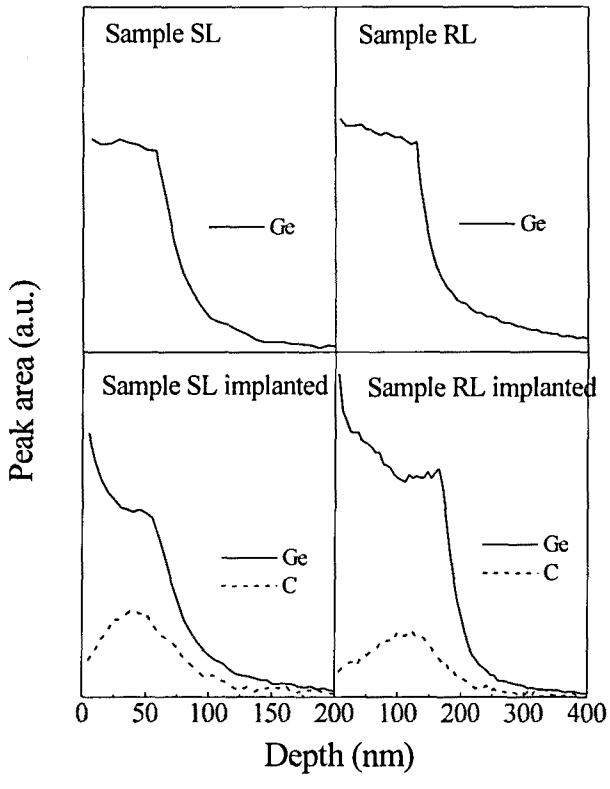

Figure 4.14 XPS profiles from the SL and RL as-grown and implanted samples.

These profiles have been obtained from the area of the Si2p, C1s and $Ge2p^{3/2}$ peaks, which have been measured on the surface of the samples after etching at different depths with a 4 keV Ar^+ beam. In both cases, the C profile from the implanted samples shows a skewed gaussian shape, which is related to the implantation process. The Ge profile is no longer constant throughout the layer and it presents a minimum in the region corresponding to the maximum concentration of C. This indicates the existence of a Ge diffusion process from the implanted region, where C precipitates in the form of β-SiC, towards the SiGe regions above and below the implanted peak. This enhanced diffusion is related to the phase separation induced by the implantation process. During implantation, C atoms tend to precipitate in the form of β-SiC, and Ge atoms are ejected from this region. This fact is similar to the amorphous SiGe case previously presented.

Figure 4.15 shows the TEM images and the corresponding TED patterns of the RL sample, before and after the implantation. For the as-grown sample, the TED pattern shows the splitting of the diffraction spots corresponding to the epitaxial layer and to the substrate. After the implantation, it is clear from the image that a high density of precipitates has been formed, which are identified as β-SiC from the TED pattern. These precipitates are seen in the image as bright spots, which contain Moiré fringes, and extend from about 60 to 135 nm. From the distribution of the β-SiC spots and from the Moiré fringes in the figure, a well-defined orientation relationship between the SiC the SiGe lattices can be deduced confirming the data already reported from XRD. This result proves that phase separation occurs during a very high dose implantation: the C atoms tend to precipitate in the form of β-SiC, and in this process Si from the $Si_{0.55}Ge_{0.45}$ is consumed, what causes a Ge enrichment of the layer. This behaviour is similar to that observed in amorphous implanted SiGe layers (discussed in previous sections). The Ge enhanced diffusion has also been reported in the literature[20] from Si/SiGe/Si metastable structures grown by RTCVD, where SiC precipitation is induced by thermal annealing. A confirmation of this mechanism is provided by the larger separation of the $Si_{1-x}Ge_x$ with respect to the as-grown sample and the appearance of Si spots in the TED pattern of the figure. Furthermore, the surface becomes slightly wavy, with a roughness of about 3 nm. In this sample, the C profile did not reach the interface between the layer and the substrate and the interface remains clearly visible.

Figure 4.16 shows the TEM images of the SL as-grown sample before and after implantation. In this case, the splitting of the diffraction spots cannot be seen in the as-grown sample, because of the lower Ge content. Again the presence of β-SiC precipitates can be seen in the TEM image, and the orientation relationship is the same as for the RL sample, as well as for the Si implanted wafers. In this image, the interface $Si/Si_{1-x}Ge_x$ appears to be strongly damaged by the implantation, although it can still be identified. This is due to the penetration of the implanted tail in the Si substrate region, as shown in the TRIM profile from figure 4.11. The presence of a damaged region below the implanted peak was already observed in the Si implanted wafers, as discussed in chapter III. This is related to the accumulation of self-interstitials in this region, which can not relax in the surface of the sample. In this case, a higher density of defects is to be expected, due to the relaxation of the SiGe region below the implanted peak. Anyway, it is interesting to remark the improvement in the structural quality of the β-SiC grains, which is determined by their growth under the compressive strain of the epitaxial SiGe lattice. This is observed from the decrease in the residual tensile strain of the β-SiC grains, and from their degree of missorientation in relation to the target lattice, when compared to the SiC crystal synthesised in a Si wafer by an equivalent implantation, as shown in table IV-III.

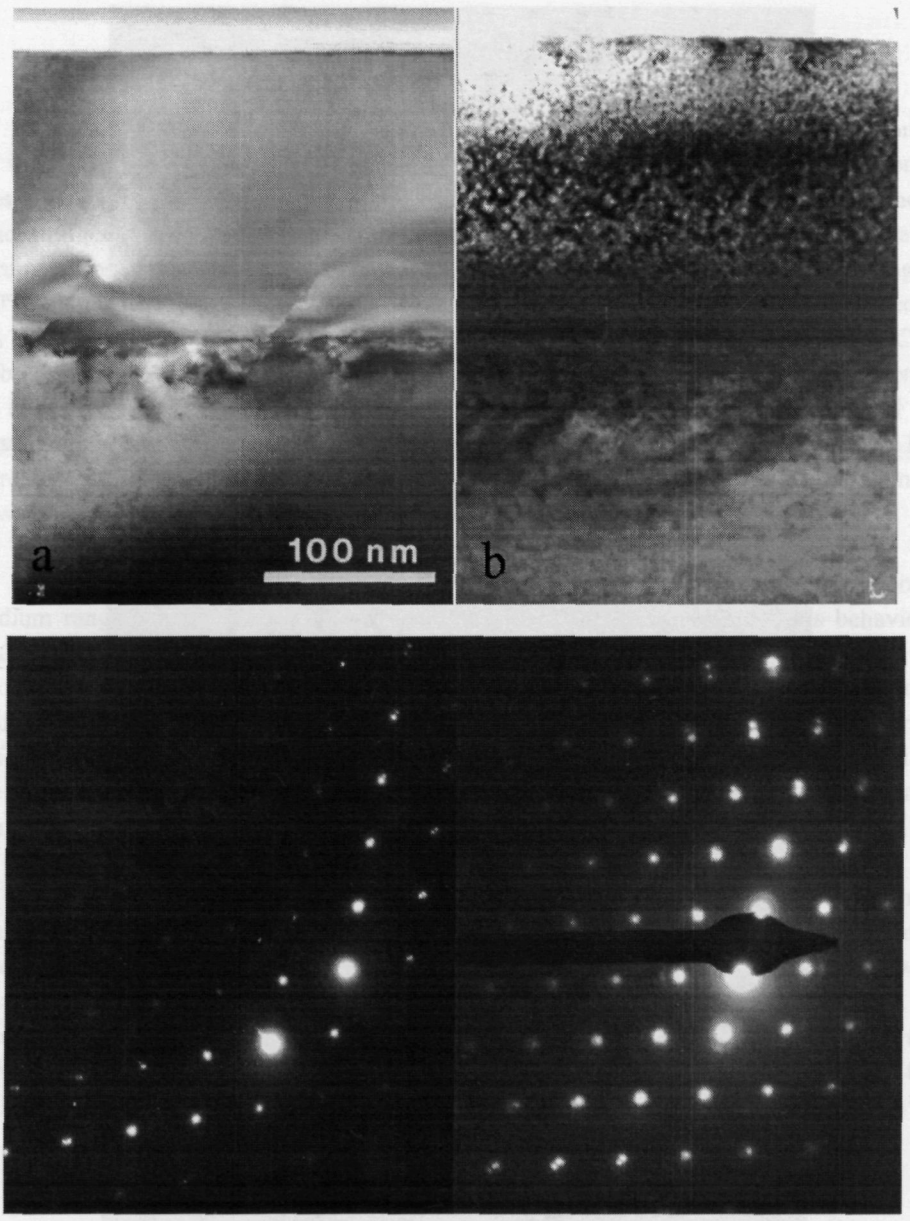

Figure 4.15 TEM of RL sample (a) as grown and (b) and implanted. TED of the same samples is below each one.

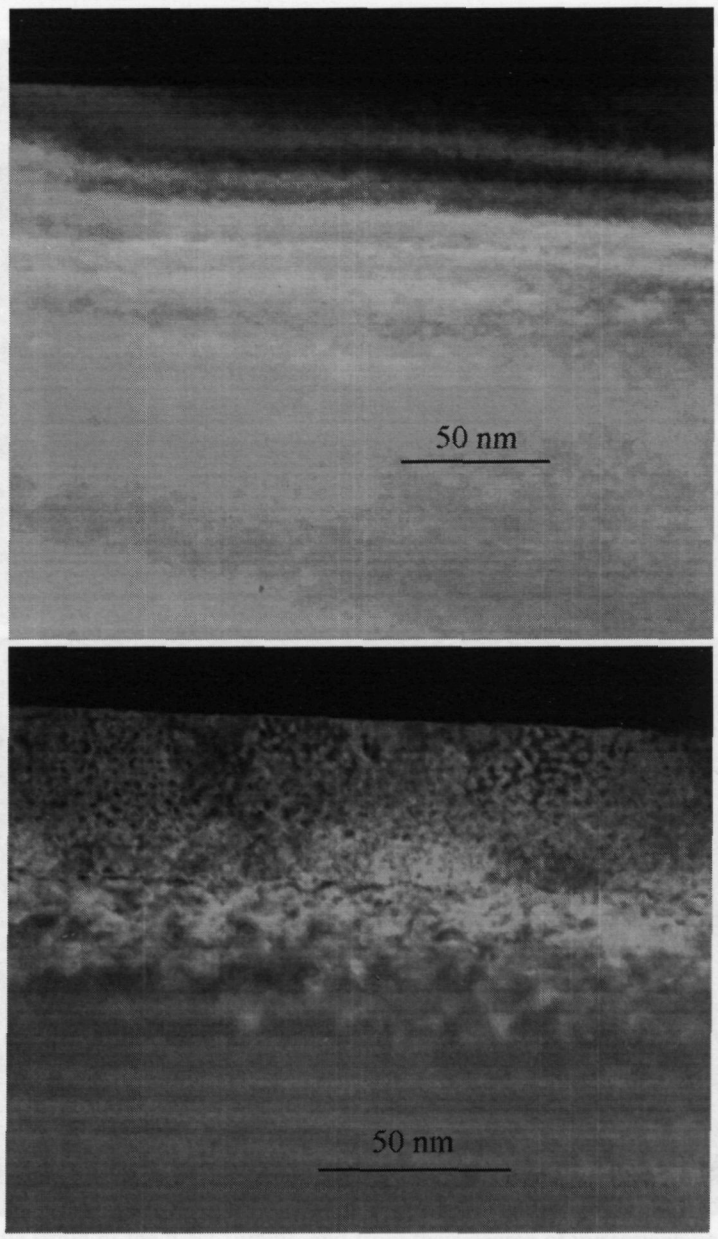

Figure 4.16 TEM image of a SL sample as-grown (top) and implanted (bottom).

4.4 CONCLUSIONS

SiGe/SiC structures have been synthesised by medium to high dose C implantation at RT in $Si_{1-x}Ge_x$ amorphous layers. All the obtained data imply that both the C incorporation in substitutional sites in the network and the formation of SiC crystals are determined by the C concentration present in the samples. For concentrations lower than 1-2%, C preferably occupies substitutional places and the formation of SiC is not observed even annealing at 900°C, although a decrease in the C substitutional incorporated to the network is detected at this temperature. For higher concentrations up to 15%, there is coexistence between C in susbtitutional places and highly distorted SiC crystalline. An increase in the C concentration in the implanted region up to a maximum of 37% drives forward a drastic improvement of the crystallinity in the SiC grains, together with an absence of any C substitutional signal. The correlation of these data with those about microstructure suggests that the incorporation of substitutional C is related to the SPE recrystallisation of the amorphous Si substrate.

With respect to the improvement in crystalline quality, implanting at a concentration of medium range (up to 10%), the growth of SiC precipitates is distorted. This behaviour could be related to the formation of C aggregates and Si interstitials, as a step between the incorporation of C substitutional to the Si network and the growth of SiC grains. Raman results suggest that the C incorporation takes place in a preferred way in the Si substrate which epitaxially recrystallises. The absence of C incorporated in the SiGe grains could be due to the higher distortion around a C substitutional in the SiGe lattice than in the Si one, due to the higher lattice parameter of SiGe.

On the other hand, the characterisation of high temperature C implantation into strained and relaxed epitaxial $Si_{1-x}Ge_x$ layers has been performed. The different implanted doses have been selected to obtain a peak C concentration similar to the Ge content, x, well above the C content obtained in metastable binary and ternary layer. For these conditions no C is detected in substitutional positions in the layer, and a phase segregation and the formation of β-SiC crystalline grains oriented in relation to the implanted lattice with the well-known relationships of $[001]_{SiC}\|[001]_{Si}$ and $(110)_{SiC}\|(110)_{Si}$ are observed.

The comparison between the SiGe epitaxial implanted layers and the equivalent implanted Si wafers indicates the existence of significant differences, which are related to the lattice constant and the strain in the target lattice. For the SiGe relaxed lattice, there is an increase in the residual tensile strain in the SiC grains, which is caused by the higher free volume produced by the injection of interstitials, mainly Ge atoms, from the implanted region. The higher elastic distortion of the crystals is also accompanied by a higher degree of missorientation in relation to the host lattice. This contrasts with the behaviour of the SiGe fully strained layer. In this case, the growth of the SiC crystals occurs under a biaxial compressive strain, which partially compensates the residual tensile strain, thus improving the crystalline orientation of the β-SiC crystals in relation to the target lattice.

In all the observed cases (RT implantation into SiGe amorphous layers and high temperature implantation into epitaxial $Si_{1-x}Ge_x$ single crystal layers), the formation of SiC is accompanied by a strong Ge enhanced diffusion from the implanted peak. This is related to the higher stability of SiC, in relation to the formation of Ge-C bonds. Diffusion from the implanted peak in the epitaxial layers gives rise to a significant Ge enrichment in the SiGe regions above and below the implanted peak, where there is a maximum content of SiC grains, which determines relaxation of the SiGe lattice from the fully strained sample.

4.5 REFERENCES

1. O. González-Varona,
M. D. Thesis, University of Barcelona (1998)

2. *Enclyclopedia of Materials Characterisation*, Eds. C. R. Brundle, C. A. Evans, S. Wilson Butterworth-Heinemann, Stoneham (1992)

3. *Semiconductor Science: Growth and Characterisation,* Eds. T. E. Jenkins, T. Jenkins Prentice Hall, New York (1995)

4. L. Vegard
Z.Phys. *5* p. 17 (1921)

5. S. C. Jain, H. J. Osten, B. Dietrich, H. Rücker
Semiconductors Science and Technology *10* p. 1289 (1995)

6. P. C. Keriles
Physical Review Letters *75* p. 1114 (1995)

7. D. H. Whysong
Journal of Undergraduated Researcher Physics *12* p. 51 (1994)

8. M. Melendez-Lira, J. Menendez, W. Windl, O. F. Sankey, G. S. Spencer, S. Sego, R. B. Culbertson, A. E. Bair, T. L. Alford
Physical Review B *54* p. 12866 (1996)

9. *Annual book of ASTM Standards*, ASTM
ASTM, Philadelphia (1996)

10. M. Melendez-Lira, J. Menendez, K. M. Kramer, M. O. Thompson, N. Cave, R. Liu, J. W. Christiansen, N. D. Theodore, J. J. Candelaria
Journal of Applied Physics *82/9* p. 4246 (1997)

11. K. E. Erberl, S. S. Lyer, S. Zollner, J. C. Tsang, F. K. Le Goues
Applied Physics Letters *64* p. 3033 (1994)

12. H. J. Osten, E. Bugiel, P. Zaumseil
Applied Physics Letters *64* p. 3440 (1994)

13. B. Dietrich, H. J. Osten, H. Rücker, M. Methfessel, P. Zaumseil
Physical Review B *49* p. 17185 (1994)

14. J. Menendez, P. Gopalan, G. S. Spencer, N. Cave, J. W. Strane
Applied Physics Letters *66* p. 1160 (1995)

15. J. W. Strane, S. R. Lee, H. J. Stein, S. T. Picraux, J. K. Watanabe, J. W. Mayer
Journal of Applied Physics *79* p. 637 (1996)

16. A. Chehaidar, R. Carles, A. Zwick, C. Meunier, B. Cros, J. Durand
Journal of Non-Crystalline Solids *169* p. 37 (1994)

17. J. Desseaux-Thibault, A. Bourret, J. M. Penisson
Institute of Physics Conference Series *67/2* p. 71 (1983)

18. H. Bender, J. Vanhellemont
Physica Status Solidi A *107* p. 455 (1988)

19. A. De Veirman
Ph. D. Thesis, University of Antwerpen (1990)

20. P. Warren, J. Mi, F. Overney, M. Dutoit
Journal of Crystal Growth *157* p. 414 (1995)

21. J. W. Strane, H. J. Stein, S. R. Lee, S. T. Picraux, J. K. Watanabe, J. W. Mayer
Journal of Applied Physics *76* p. 3656 (1994)

22. M. Matthews
Journal of Vacuum Science and Technology *12* p. 126 (1975)

23. A. Nejim, P. L. F. Hemment, J. Stoemenos
The Electrochemical Society Proceedings *94-11* p. 167 (1994)

CHAPTER 5

GENERAL CONCLUSIONS

i) The study of ion beam amorphised 6H-SiC has allowed to observe the absence of a complete chemical order. The Raman spectra are characterised by the presence of broad bands related to the Si-Si and C-C vibrational modes. The shape and position of the C-C mode suggests the existence of a mixed sp^2-sp^3 complex hybridation. The absence of an epitaxial recrystallisation of the ion beam amorphised layers is inferred from the presence of these highly stable C-C bonds. Thus, it is necessary to avoid amorphisation when doping by ion implantation SiC, which in principle can be achieved by implanting at temperatures higher than RT.

ii) The analysis of ion beam amorphised 6H-SiC has been extended to the study of the effect of the temperature of implantation in wafers implanted with Al^+ ions. The implantation conditions have been chosen in order to obtain a 400 nm thick layer with a constant Al content of about $5x10^{19}$ cm^{-3}. The study shows that there is a strong dependence of the ion beam induced damage on the implantation temperature. The amorphisation of the implanted layer has been avoided by implanting at temperatures of 200°C or higher. For implantation temperatures below 1000°C, damage in the implanted layer decreases as the implantation temperature increases. A saturation of damage occurs for higher temperatures of implantation. This phenomenon could be explained by the formation of extended defects, which requires the mobility of point defects (vacancies and interstitials) that takes place at implantation temperatures higher than 1000°C. An annealing at 1500°C leads to a similar level of residual damage, concluding again that amorphisation of the implanted layer has to be avoided.

iii) The detailed structural characterisation of ion beam synthesised amorphous SiC has been completed with the analysis of layers obtained by high dose C ion implantation into premaorphised Si targets. This has corroborated the existence of an intermediate situation between the perfect mixing and the complete chemical order in amorphous $Si_{1-x}C_x$. For the composition range $0.35 < x < 0.6$, there is a saturation in the percentage of heteropolar bonds at 70%. In all the range of compositions analysed, the XPS analysis indicates the presence of two main contributions in the Si2p and C1s spectra, corresponding to the $Si\text{-}Si_4$ and $Si\text{-}C_4$ tetrahedral bonds in the Si2p spectra, and to the corresponding $C\text{-}Si_4$ and $C\text{-}C_4$ configurations in the C1s spectra. This shows a clear trend of the amorphous network towards partial chemical ordering with phase separation, instead of homogeneous dispersion.

iv) Moreover, the in-depth analysis of the Si wafers implanted with C^+ ions at RT reveals the existence of two competitive mechanisms that take place during the implantation process, that is the formation of a SiC buried layer and the C migration towards the surface. Thermal annealing at temperatures T>900ºC allows the recrystallisation of SiC in the form of randomly oriented β-SiC nanograins, and the disappearance of the C peak at the surface. However, the recrystallisation of the SiC amorphous layer is compromised by the high stability of the C-C bonds. The C-C Raman band evolves from a mixed sp^2-sp^3 co-ordination to a highly stable graphitic sp^2 one. This causes the presence of a residual amorphous graphitic C in the samples, probably located at the intergrain regions. No significant improvement in the crystalline quality of the samples has been observed when annealing by IBIEC processes instead of by thermal recrystallisation at 1150ºC.

v) The detailed analysis of Si wafers implanted with C^+ ions at 500ºC shows the direct formation of a buried layer with β-SiC crystalline precipitates, with sizes in the range of 7-10 nm and the same crystalline orientation than the Si network. An annealing at 1150ºC produces an increase in the crystalline quality of both the Si and SiC crystalline phases. The dominance of the direct synthesis of crystalline SiC, according to a topotactic transformation from the cubic Si lattice to the cubic β-SiC one, probably avoids the C diffusion towards the surface. In spite of the very high lattice mismatch between both lattices, the SiC grains in the as-implanted structures have residual strain of tensile character in the order of 0.1-1%. This strain relaxes in a significant way after the annealing. This has been related to the existence of a very thin amorphous-like interface surrounding the SiC grains. The nature of this interface is not clear, although the spectroscopic data suggests that it is not related to the excess of C.

vi) The etch-stop behaviour of the implanted layers with TMAH etchant solutions has been analysed. TMAH has been chosen because of its higher compatibility with CMOS technology than other Si anisotropic etchants. The results obtained indicate the existence of a minimum C content of about $1.7x10^{22}$ cm^{-3}, which is needed to achieve an efficient etch-stop behaviour. Below this value, no significant differences has been found in the etch-rate of the implanted layers in relation to that measured in not processed virgin Si wafers. By implanting at doses leading to C contents above this value, no appreciable etching of the implanted layer is observed, even for the longest etching times of 1 hour. This behaviour has been interpreted in terms of a percolation model, assuming a binary Si/SiC structure of the implanted layer.

vii) A buried stoichiometric β-SiC layer with abrupt interfaces with the top Si and substrate regions has been synthesised by a 4-step implant process. This layer has been successfully applied for obtaining simple micromechanical test devices. The high structural quality of the synthesised layers with its extreme etching selectivity, together with the abruptness of both Si/SiC interfaces and the low residual strain after the annealing have allowed the fabrication of self-standing test structures such as membranes, bridges and cantilevels. The high stiffness of SiC permitted the fabrication of beams as long as 100 μm and up to 40 μm wide, in spite of their low thickness (of about 300 nm). These layers can also be used as seed for growing thicker SiC films, with potential advantages in relation to the thin carbonised layer used in the CVD growing of SiC in Si.

viii) SiGe/SiC polycrystalline structures have been synthesised by medium to high dose C^+ ion implantation into SiGe amorphous layers and afterwards annealed. The C content in the implanted region strongly determines its structure. At low C contents, below 1-2%, C is preferentially located at substitutional sites and no SiC formation is detected even after annealing at 900°C. The recuperation in the Si lattice is enhanced by the Solid Phase Epitaxial (SPE) regrowth. For intermediate doses, leading to C contents up to about 15%, both substitutional C in the Si lattice and highly distorted SiC crystals are observed. In both cases, substitutional C is preferentially located at the Si network, which is probably related to the higher local distortion around substitutional C atoms in the SiGe lattice. The increase of the implanted dose up to a peak C content of 37% drives forward a drastic improvement of the crystallinity of the SiC grains, and no signal from substitutional C in the Si or SiGe lattices is found at all.

ix) Crystalline SiC grains have also been directly synthesised by implanting strained (x=0.27) and relaxed (x=0.56) epitaxial $Si_{1-x}Ge_x$ layers. The implantation conditions were selected to obtain a peak C content similar to the Ge content, x. According to the previous results from RT implantation into amorphous substrates, these doses are far above the values expected for the formation of metastable $Si_{1-y}C_y$ or $Si_{1-x-y}Ge_xC_y$ alloys. For these conditions, substitutional C in the binary or ternary alloy is not detected, and phase segregation and the formation of β-SiC grains with the same crystalline orientation than the host lattice is observed. In comparison with the equivalent implantions on single crystal Si substrates, an increase in the residual strain of the SiC grains is observed from the $Si_{1-x}Ge_x$ relaxed layer. This is probably related to the higher free volume produced by the injection of interstitials, mainly Ge atoms, from the implanted region. The higher elastic distortion of the crystals is also accompanied by a higher degree of missorientation of the crystals. This contrasts with the behaviour from the fully strained layer. In this case, a strong Ge enhanced diffusion from the implanted peak and a Ge enrichment of above and below the SiGe regions occur, which relaxes the fully strained SiGe sample.

x) Finally, in all cases (RT implantation of amorphous SiGe substrates or high temperature implantation of $Si_{1-x}Ge_x$ crystalline layers) the formation of SiC is acompanied by a strong Ge enhanced diffusion from the implanted layers. This is related to the higher stability of the Si-C bond, in relation to the Ge-C one, and leads to complex SiGe/SiC multilayer structures. For the implanted $Si_{1-x}Ge_x$ strained layer, the Ge enrichment in the SiGe lattice determines its strain relaxation. These data point out the strong trend of the implanted systems towards phase separation into both SiGe and SiC lattices.

RESUMEN

1. Introducción

El Carburo de Silicio (SiC) es un compuesto térmica y químicamente estable cuyas excelentes propiedades físicas vienen siendo aplicadas con éxito en diversos campos para la fabricación de dispositivos electrónicos y sistemas micromercánicos. Aunque de procesado bastante complejo, debido a su tendencia a cristalizar en distintas fases o politipos, las características electrónicas del SiC hacen de él un material interesante para su utilización en dispositivos que trabajen en entornos agresivos y condiciones extremas. Continuamente surgen prometedoras aplicaciones que estimulan los esfuerzos de desarrollo y mejora de métodos de crecimiento de este material, tanto en volumen como en capas sobre un substrato adecuado.

Los dispositivos electrónicos formados por SiC pueden operar a temperaturas muy altas sin sufrir efectos de conducción intrínseca, gracias a su gran gap de energía. Su excelente estabilidad química permite trabajar en entornos químicamente agresivos incluso bajo radiaciones extremas. Además, el SiC puede aguantar campos eléctricos elevados sin sufrir roturas por avalancha, lo que permite la fabricación de diodos y transistores de muy alto voltaje y alta potencia. Adicionalmente, la densidad de empaquetado de estos dispositivos puede ser muy alta, algo muy necesario en tecnologías de circuitos integrados. Por otro lado, el SiC es un conductor térmico excelente lo que permite obtener dispositivos que disipan con facilidad los grandes excesos de calor generados por la electrónica adicional. Los dispositivos de SiC también pueden operar a muy altas frecuencias (microondas). En conjunto estas propiedades hacen que los dispositivos basados en SiC ofrezcan enormes beneficios en un gran número de aplicaciones industriales, con respecto a los basados en otros semiconductores disponibles. Dentro de las numerosas aplicaciones electrónicas del SiC, cabe mencionar los dispositivos optoelectrónicos, de alta temperatura, de radiaciones extremas, de alta potencia y de alta frecuencia, como LEDs de tres colores, MOSFETs de potencia, transistores bipolares, fotodiodos y rectificadores que están siendo comercializados por distintas compañías internacionales.

Por otra parte, la rigidez mecánica del SiC y su modulo de Young, superior al del Si, hacen que este material sea especialmente adecuado para la obtención de dispositivos y sistemas en tecnologías micromecánicas. En este sentido, el SiC es un candidato ideal para el desarrollo de sistemas Micro-Electro-Mecánicos (MEMS) que tengan que trabajar en ambientes agresivos, tanto desde el punto de vista térmico (alta temperatura) como químico o bajo radiaciones intensas. En este campo, se han desarrollado diferentes tipos de sensores basados en SiC, como sensores de gas a partir de dispositivos MOSiC, o sensores de presión piezoresistivos, y se está estudiando la integración del SiC como capa activa o de soporte en una amplia gama de dispositivos.

2. Síntesis por implantación iónica de SiC

La síntesis a gran escala de SiC, con calidad y pureza suficientes para su uso en las aplicaciones ya citadas, no se puede realizar a través de procesos de sublimación y de crecimiento en vapor. A pesar de los numerosos estudios llevados a cabo y de los avances en el terreno de crecimiento de SiC cristalino en volumen, el material así obtenido contiene una gran densidad de defectos y su precio, una vez procesado, es aún demasiado alto.

Por ello, el crecimiento de capas de SiC cristalino sobre otros substratos constituye un acercamiento interesante al problema. Obtener capas de SiC sobre Si, el material semiconductor por excelencia, no es tan caro y sí puede ser especialmente útil, pues resultará trivial compatibilizar los procesos del SiC así obtenido con la tecnología de Si. En la actualidad, las técnicas más utilizadas son el depósito químico en fase vapor (CVD) y la epitaxia por haces moleculares (MBE), siendo normalmente necesaria una etapa previa de carbonización de los substratos. Estas técnicas pueden presentar problemas, debido a la posible degradación de la calidad cristalina de las capas de SiC, motivada por el elevado desapareamiento de red entre Si y SiC, así como por la formación de cavidades en la interficie SiC/Si, producidas por la gran afinidad del Si para enlazarse con el C. Esto implica la necesidad de optimizar los procesos, que normalmente involucran temperaturas elevadas, lo que impone limitaciones importantes en cuanto a su versatilidad.

Todo esto contrasta con la implantación iónica que, en combinación con procesos de recocido, constituye una alternativa interesante para la síntesis de capas de SiC. La mayor versatilidad de estos procesos, que son en principio compatibles con la tecnología estándar de Si, junto con su facilidad de control, permite abordar la fabricación de estructuras multicapa complejas.

La calidad del material sintetizado por implantación iónica depende fuertemente de las condiciones de implantación y recocido, lo que implica la necesidad de optimizar los parámetros tecnológicos propios de la implantación, así como del diseño de proceso. El estudio de la implantación de C en Si se puede separar en tres áreas en función de la cantidad de C introducido, según la cantidad sea igual o inferior al límite de solubilidad del C en Si, sea mayor que ese límite pero menor que la concentración necesaria para formar SiC estequiométrico, o sea mayor que esta concentración.

Si se introduce una cantidad de C inferior o del orden del límite de solubilidad sólida en equilibrio, el C tiende a incorporarse en la red de Si ocupando principalmente posiciones sustitucionales, aunque la distorsión de la red y la presencia de defectos puede privilegiar otras configuraciones. Para difundir de estas posiciones se necesitan defectos puntuales, si bien los procesos de difusión parecen ser independientes de la concentración de C. La precipitación de C en forma de SiC se produce o bien en entornos de sobresaturación de Si intersticiales, o vía aglomerados de C, dependiendo de la características de la red implantada y del proceso. Ambos procesos conllevan una reducción de volumen o contracción de la red y la absorción de Si intersticial o emisión de vacantes de Si.

Cuando la concentración de C introducido se encuentra por encima del límite de solubilidad sólida, pero por debajo de la relación estequiométrica del SiC el comportamiento del C implantado es variado e interesante. A estas concentraciones el dañado que produce la implantación puede afectar profundamente el tipo de incorporación del C, pudiendo predominar el C en posiciones intersticiales. El confinamiento de dicho dañado también afecta a la reconstrucción epitaxial del Si tras un proceso de recocido, para capas amorfizadas por la implantación iónica. Las capas en que se encuentra la mayor parte del C enterrado son ricas en microregiones de SiC, que se aglomeran tras un adecuado proceso de recocido. A partir de un punto en que la precipitación de C en forma de SiC es suficientemente pronunciada, el crecimiento epitaxial tras un proceso de recocido se inhibe, pudiendo producirse una redistribución del C, que contribuye a la relajación de la red relocalizando los átomos de Si desplazados y formando capas continuas de SiC. Por otro lado, la superficie del material se revela como una región que condensa parte del C enlazado principalmente a si mismo.

Cuando la concentración del C implantado es mayor que la dosis umbral necesaria para formar capas de SiC, éstas se consiguen fácilmente en superficie o enterradas. La forma cúbica β-SiC es la estructura de equilibrio resultante de la transformación topotáctica impuesta por la red de Si. La microestructura de las capas sintetizadas depende de forma crítica de la temperatura de implantación y de la de recocido. Los enlaces de C-C se ven favorecidos energéticamente con el exceso de C implantado.

A partir de la síntesis de SiC en Si, se han escogido también otro tipo de materiales como substrato, que pueden aportar nuevas y mejores características, como por ejemplo capas de $Si_{1-x}Ge_x$ crecidas sobre Si. Este tipo de estructuras permiten nuevos grados de manipulación de las propiedades mecánicas y eléctricas. La tensión inherente de las capas de SiGe sobre Si afectará fuertemente a la estructura de bandas electrónicas, y con ello a las propiedades eléctricas del material. Procesos de relajación de este tipo de tensiones se pueden producir con la incorporación de C en estas capas, formando o no SiC.

3. Objetivos

El objetivo principal de este trabajo es el estudio de la síntesis por implantación iónica de SiC en substratos de Si y estructuras SiGe/Si. Para ello se desarrolla una completa caracterización estructural y físico-química de los distintos procesos, a la vez que se aborda la obtención de un material utilizable como base para la realización de dispositivos micromecánicos simples.

El estudio realizado se ha estructurado en tres partes. La primera parte está dedicada a la síntesis y recristalización de capas de SiC amorfo. Como paso previo a dicha síntesis, se ha caracterizado el comportamiento de 6H-SiC comercial frente a procesos de implantación, valorando el papel que juegan la dosis y temperatura de implantación, y la temperatura de recocido. Una vez realizada esta caracterización, se ha abordado el estudio de capas de Si amorfo implantadas con iones de C a temperatura ambiente (RT), estudiando en detalle la disposición de los enlaces químicos existentes en función del contenido de C introducido. Posteriormente, se ha considerado la recristalización de este material tanto térmicamente como por IBIEC (cristalización epitaxial inducida por haces iónicos).

En la segunda parte se ha tratado la síntesis directa de SiC cristalino. Para ello se han realizado los procesos de implantación a una temperatura suficientemente elevada como para evitar la amorfización del substrato. Eso se puede conseguir utilizando temperaturas de implantación moderadamente altas. Así, una temperatura de implantación de 500°C ha sido suficiente para mantener la cristalinidad del substrato. Esta parte se inicia con el estudio de procesos de implantación a dosis subestequiométricas (inferiores a la dosis umbral necesaria para la obtención de una composición SiC estequiométrica en el máximo de la implantación). Esto ha permitido caracterizar los procesos fundamentales involucrados en la síntesis por implantación iónica de SiC cristalino.

Posteriormente, se ha definido un proceso de implantación múltiple que ha permitido sintetizar una capa continua y estequiométrica de SiC enterrada en el substrato de Si. La caracterización de las muestras implantadas ha corroborado la formación de esta capa, con interficies abruptas con la región superficial y el substrato de Si. Esta parte finaliza con el estudio detallado de las propiedades de paro de ataque químico (etch-stop) de las capas implantadas. La excelente selectividad al ataque químico entre estas capas y las regiones de Si ha permitido la fabricación de estructuras de test micromecánicas, como membranas, puentes y otras estructuras simples. La realización de este tipo de estructuras, a partir de las capas sintetizadas por implantación iónica, constituye uno de los principales objetivos alcanzados en este trabajo, demostrando la viabilidad de los procesos de micromecanizado de las capas.

Por último, la tercera parte del trabajo está dedicada al estudio de los procesos de implantación en capas de SiGe. Este estudio tiene como objetivo investigar la dependencia de las fases sintetizadas en el proceso de implantación de parámetros del substrato como el estrés, la composición química y la constante de red. También se plantea la posible modificación de las fases sintetizadas por la incorporación de tomos de Ge, dando lugar a aleaciones ternarias $Si_{1-x-y}Ge_xC_y$. Este estudio se desarrolla de forma similar al trabajo realizado previamente en Si. En una primera fase, se plantea la síntesis y recristalización de capas amorfas, pasando en una etapa posterior al estudio de procesos a temperaturas elevadas (500°C) en capas epitaxiales.

4. Técnicas de análisis y caracterización

Con el fin de caracterizar adecuadamente los materiales estudiados en este trabajo se han utilizado distintas técnicas de caracterización entre las que destacan las espectroscopías Raman y FTIR, junto con XPS y TEM. La mayoría de los equipos científicos utilizados forman parte de la infraestructura tecnológica perteneciente a la Universidad de Barcelona y emplazada en los Servicios Científico-Técnicos creados por dicha universidad con el fin de apoyar la investigación científica.

Las espectroscopías Raman e infraroja (FTIR) son técnicas vibracionales no destructivas muy útiles en la caracterización de estructuras y procesos en tecnologías de Si. La espectroscopía Raman aporta información estructural sobre el carácter amorfo o cristalino de las muestras, además de permitir el estudio sobre defectos, tensiones y desorden en las capas estudiadas.

La espectroscopía Raman es más sensible a los parámetros relacionados con el enlace químico que a la relación de composición química entre elementos o enlaces, o a la detección de trazas de impurezas. La técnica FTIR complementa el análisis estructural en aquellas capas que presentan una baja eficiencia en Raman, por ejemplo en capas dieléctricas de SiO_2 o Si_3N_4, y constituye una técnica especialmente adecuada para el estudio de la formación de SiC.

Las técnicas de emisión de electrones, basadas en medidas de la distribución de energía de los electrones emitidos por un material, proporcionan una rápida identificación atómica y permiten determinar el estado químico (o enlace) del átomo. Estas técnicas de UHV son de análisis superficial, debido al corto trayecto medio del electrón libre, aunque combinadas adecuadamente con un cañón de iones que realice un cráter en la muestra se pueden obtener análisis por debajo de la superficie y conseguir perfiles de concentración elementales en profundidad. La espectroscopía de fotoelectrones (XPS o ESCA) es muy útil en los estudios de composición química. La espectroscopía Auger (AES) se utiliza con frecuencia para una rápida detección elemental y seguimiento de profundidad, siendo sus principales ventajas con respecto a XPS la mejor resolución tanto lateral como en profundidad, y su principal desventaja la práctica imposibilidad de estudiar materiales aislantes y de determinar adecuadamente gran parte de los enlaces químicos de los elementos detectados.

Las microscopías electrónicas se utilizan exhaustivamente en el estudio estructural de materiales sólidos, ofreciendo una imagen altamente magnificada con buena resolución lateral. En microscopía de transmisión (TEM) se pueden conseguir aumentos del orden de 10^6, permitiendo determinar defectos presentes en el material, y el estudio de los patrones de difracción de los electrones (TED) permite caracterizar el estado y la estructura cristalinas de las capas.

En contraste con TEM, que requiere de técnicas complejas para la preparación de las muestras, la microscopía electrónica de barrido (SEM) prácticamente no requiere preparación de las muestras. Unicamente en el caso de muestras aislantes se hace necesario su recubrimiento con una fina capa metálica para prevenir la acumulación de carga. Esta técnica ha sido utilizada fundamentalmente para la observación de las estructuras micromecánicas realizadas en las capas implantadas.

Otras técnicas adicionales se han utilizado para completar el análisis de las muestras. Estas incluyen técnicas como la Difracción de Rayos X, para caracterizar la tensión residual en los cristales de SiC, así como su orientación cristalina en relación con el substrato implantado.

Medidas de espectrometría de masas de iones secundarios (SIMS) han sido también utilizadas de forma complementaria a las técnicas de XPS y AES para la determinación de los perfiles de iones implantados. Por otra parte, la espectroscopía Rutherford Backscattering (RBS) ha permitido estudiar la amorfización y recristalización de estructuras SiGe/Si en función de la dosis de implantación y la temperatura de recocido. Finalmente, se han realizado medidas de rugosidad superficial con un microscopio de fuerzas atómicas (AFM), una técnica perfilométrica tridimensional de muy alta resolución (0.1 A) y no destructiva. La siguiente tabla es un resumen de las características fundamentales de las diferentes técnicas utilizadas.

TECNICA	INFORMACION OBTENIDA	ALCANCE EN PROFUNDIDAD	RESOLUCION LATERAL.	DESTRUCTIVA
Raman	Estructura	0.1-10μm	0.5-1μm	No
FTIR	Estructura Impurezas	100μm	≈cm	No
XPS	Composición Estado químico	1μm (Resolución 5nm)	75μm-1mm	Si
AES	Composición	5μm (Resolución 5nm)	100A-1mm	Si
TEM	Morfología Estructura	< 2μm	2A	Si
SEM	Superficie	1μm	1nm	No
XRD	Estructura	10-100μm	mm–10μm	No
SIMS	Composición Impurezas	100μm	50nm-2μm	Si
RBS	Composición Estructura	20μm (Resolución 2nm)	1nm-10μm	No
AFM	Superficie	<A	<A-1mm	No

5. Síntesis y recristalización de SiC amorfo

5.1 Procesos de implantación en SiC cristalino (6h-SiC)

Los análisis realizados por espectroscopía Raman en muestras de 6H-SiC denotan la capacidad de esta técnica para caracterizar procesos de implantación iónica en SiC, pues es muy sensible tanto a la presencia de daño producido por la implantación como a la determinación de las fases amorfas en el volumen estudiado. Las medidas de Raman han permitido determinar la existencia de tres distintos niveles de dañado, en función de la dosis de implantación, en 6H-SiC implantado con Ge^+ a RT y 200 keV.

i) nivel bajo de dañado, a dosis por debajo de $3x10^{12}$ cm^{-2}
ii) nivel intermedio de dañado, a dosis entre 10^{13} y 10^{14} cm^{-2}
iii) formación de una capa amorfa continua, a dosis más altas que la dosis umbral de amorfización, alrededor de $2\text{-}3x10^{14}$ cm^{-2}.

Los espectros Raman de las capas de SiC amorfizadas presentan bandas anchas características que han sido atribuidas a modos de vibración Si-Si y C-C en un entorno amorfo. Este hecho claramente muestra la ausencia de un orden químico completo en un material en fase amorfa sintetizado por implantación iónica. La forma y posición del pico atribuido a enlaces C-C sugiere la existencia de una mezcla, de una hibridación compleja sp^2-sp^3 en los enlaces homopolares de C.

Mediante tratamientos de recocido térmico, se produce la recristalización y recuperación del daño en las capas implantadas. Sin embargo, las capas tratadas térmicamente muestran un nivel importante de daño residual, incluso para recocidos a 1500ºC. Esto es debido a la gran estabilidad del daño producido en la red de SiC por la implantación iónica. Para las muestras implantadas a dosis superiores al umbral de amorfización, la recristalización de la capa amorfa ocurre en forma policristalina. La ausencia de una recristalización epitaxial en fase sólida en SiC podría estar relacionada con la pérdida parcial del orden químico al formarse enlaces C-C muy estables.

Esto implica la necesidad de evitar la amorfización de las capas en procesos de dopado de SiC cristalino, lo que se puede conseguir calentando las obleas a una cierta temperatura durante la implantación. En este contexto, el estudio de los procesos de implantación en SiC cristalino ha sido extendido a la implantación de obleas 6H-SiC con iones Al^+ (para el dopado tipo p de las capas) y en función de la temperatura de implantación, en un amplio rango entre RT y 1200ºC.

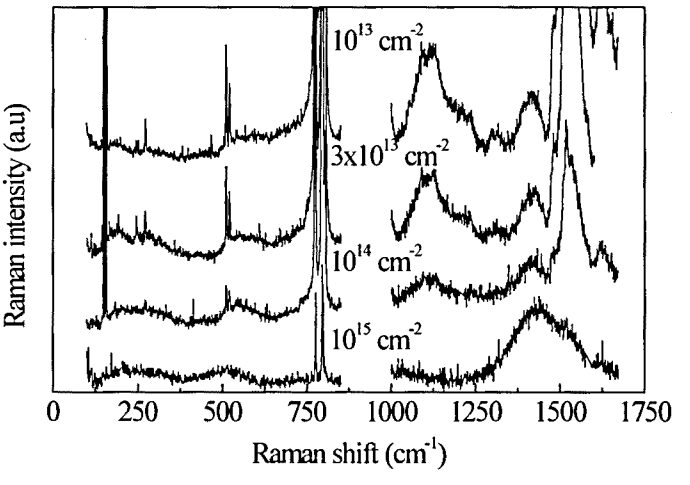

Figura 1 Espectros Raman de muestras de 6H-SiC implantadas con Ge a distintas dosis.

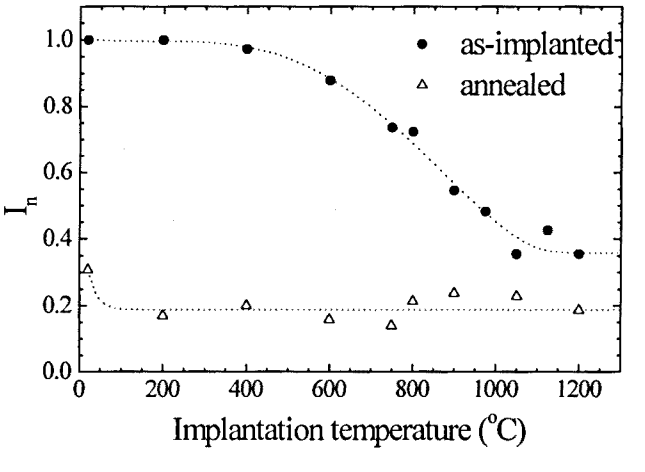

Figura 2 Intensidad normalizada relativa de la línea Raman TO en función de la temperatura de implantación para muestras de 6H-SiC implantadas con Al (capa de concentración constante 5x10^{19} cm^{-3}), antes y después del proceso de recocido a 1500°C.

Las condiciones de implantación fueron seleccionadas para obtener una capa de 400 nm de grosor con una concentración constante de Al de $5x10^{19}$ cm^{-3}, lo que ha implicado la realización de 4 etapas de implantación. Los resultados obtenidos muestran la fuerte dependencia del daño producido en el proceso de implantación con la temperatura, observando de nuevo la existencia de tres regímenes, implantación a RT para la cual se produce la amorfización de la capa implantada, implantación entre 200ºC y 1000ºC en que se observa una disminución gradual del daño con la temperatura de implantación y por último implantación a temperaturas superiores a 1000ºC, en que se obtiene una saturación del nivel de daño residual. Este comportamiento está relacionado con la estructura de los defectos creados por la implantación. Para temperaturas de implantación inferiores a 1000ºC se forman básicamente defectos puntuales, mientras que a temperaturas superiores los defectos puntuales presentan cierta movilidad que puede producir la formación de defectos extendidos.

El recocido térmico de estas muestras a 1500ºC permite obtener una recuperación significativa de la red cristalina, excepto para la muestra implantada a RT, en que se observa un daño residual importante. Estos datos se correlacionan con facilidad con el análisis eléctrico efectuado, que muestra valores de concentración de huecos y conductividad similares para todas las muestras implantadas a temperaturas suficientemente altas para evitar la amorfización. Para la muestra implantada a RT, la activación eléctrica del Al implantado se degrada debido al alto daño residual en la capa implantada.

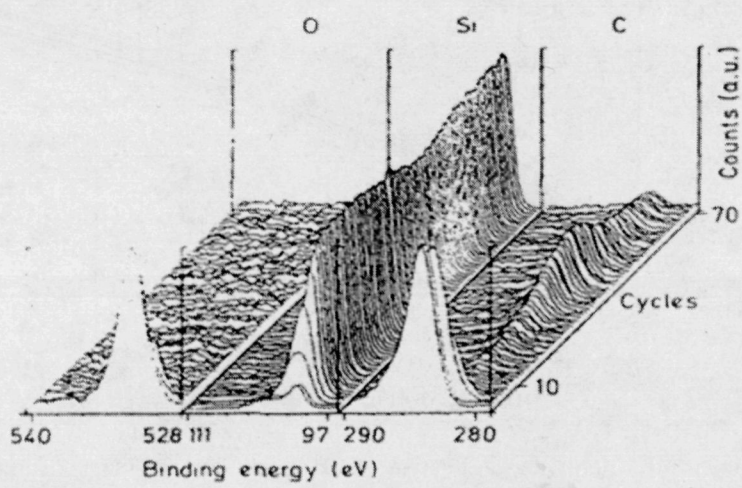

Figura 3 Perfil en profundidad de XPS de Si amorfo implantado.

5.2 Síntesis por implantación iónica y recristalización de capas de SiC amorfo en Si

Los resultados relacionados con la pérdida de orden químico obtenidos en SiC amorfizado por implantación iónica han sido corroborados en capas amorfas de $Si_{1-x}C_x$ obtenidas por implantación iónica en substratos de Si. En este caso, un estudio detallado por XPS en muestras de Si implantado con C^+ a dosis por encima del umbral necesario para una composición estequiométrica en el pico de la implantación revela la existencia de una situación intermedia entre una mezcla perfecta y un material completamente ordenado en su estructura química. Para el rango de composición $0.35<x<0.6$, existe una saturación de un 70% en el porcentaje de enlaces heteropolares, lo cual coincide con los datos de análisis de FTIR en 6H-SiC amorfizado por implantación iónica.

El análisis de los picos de XPS en función de las diferentes configuraciones de enlace tetraédrico posibles ($Si\text{-}Si_{4-n}C_n$ y $C\text{-}C_{4-n}Si_n$ con n=0-4) indican la presencia principalmente de dos contribuciones para cada pico de Si y C en todo el rango de composiciones analizadas. Estas dos contribuciones corresponden a las configuraciones $Si\text{-}Si_4$ y $Si\text{-}C_4$ en el pico de Si, y a $C\text{-}Si_4$ y $C\text{-}C_4$ en el pico de C. Este dato muestra claramente la tendencia del entorno amorfo hacia un orden químico parcial, con separación de fases, en lugar de una dispersión homogénea.

Por otra parte, el estudio de los espectros XPS obtenidos a diferentes profundidades en la muestra sugiere la existencia de dos mecanismos durante el proceso de implantación, la migración del C implantado hacia la superficie de la muestra y la formación de una capa enterrada de SiC amorfo de composición gradual. Tratamientos de recocido térmico a temperaturas superiores a 900°C producen la recristalización del SiC en la capa enterrada en forma de nanocristales de β-SiC con orientaciones cristalinas aleatorias, además de la desaparición del pico superficial de C. La recristalización de las capas amorfas de SiC se ve afectada por la alta estabilidad de los enlaces C-C que evolucionan de coordinación híbrida sp^2-sp^3 a una coordinación grafítica altamente estable sp^2. Esta fase secundaria se encuentra probablemente localizada en la zona intergranular.

Por otro lado, la recristalización epitaxial inducida por implantación iónica (IBIEC), como proceso dinámico que promueve la recristalización epitaxial a bajas temperaturas por medio de irradiación iónica, ha sido usada con el fin de recristalizar de forma alternativa las capas amorfas de SiC sintetizadas por implantación iónica en Si. Con ello se ha logrado un significativo descenso de la temperatura necesaria para la recristalización, que es de 700°C para las condiciones de radiación utilizadas (Si^+ a 300 keV y 10^{17} cm^{-2}). Sin embargo, no se ha observado ninguna mejora en la calidad cristalina de las capas recristalizadas, en relación con las muestras recristalizadas térmicamente a temperaturas superiores a 900°C.

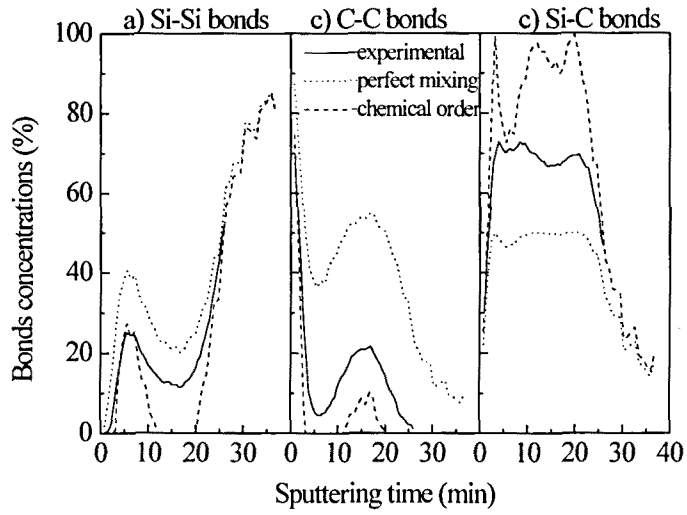

Figura 4 Perfiles de distribución relativa de enlaces Si-Si, C-C y Si-C versus tiempo de decapado, determinados por el ajuste de los espectros de XPS, y simulados asumiendo los modelos de mezcla perfecta y orden químico completo.

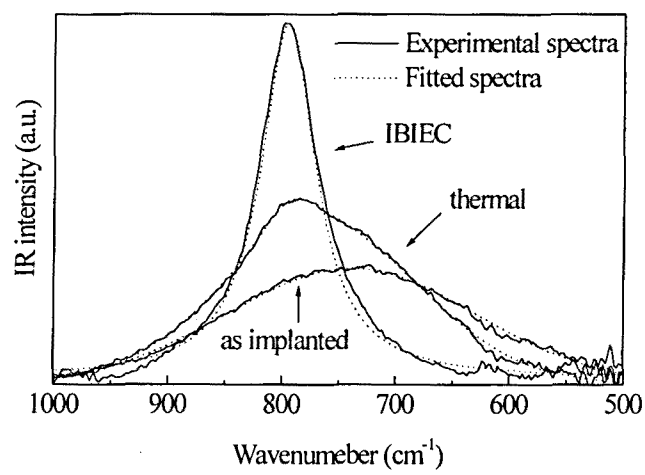

Figura 5 Espectro de FTIR de Si implantado con C, antes y después del recocido térmico y del procesado por IBIEC, junto con sus ajustes.

6. Síntesis directa de SiC cristalino

El estudio detallado de muestras de Si implantadas con iones C^+ a 500°C muestra la formación directa de una capa enterrada con precipitados cristalinos de β-SiC. Estos precipitados tienes tamaños en un rango entre 7 y 10 nm, y están orientados en la misma dirección cristalina que la red de Si del substrato. Recociendo estas estructuras a 1150°C durante varias horas se consigue una mejora en la calidad cristalina tanto del substrato de Si como de los cristales de SiC. El perfil del C implantado es muy estable bajo el tratamiento térmico y no se observa difusión de C hacia la superficie. Esto se encuentra íntimamente relacionado con el dominio de la síntesis directa de SiC cristalino, de acuerdo con la transformación topotáctica desde una red de Si cúbico a otra de SiC cúbico.

A pesar del elevado valor de desapareamiento de malla existente entre los cristales de Si y SiC, los precipitados de SiC en las muestras no recocidas presentan una tensión residual de carácter tensil, del órden de 0.1-1%. Esta tensión se relaja de forma significativa con el recocido. La observación de las muestras por HRTEM ha permitido constatar la existencia de una delgada zona interficial alrededor de los cristales de SiC, con un contraste amorfo. La naturaleza de esta zona aparentemente amorfa no está clara, aún cuando las medidas de espectroscopía Raman sugieren que no está relacionada con exceso de C. La presencia de esta envoltura aparentemente amorfa alrededor de los cristales de SiC permite explicar los bajos valores de tensión residual en los precipitados, muy inferiores a la tensión esperada a partir del desapareamiento entre las redes de Si y SiC.

Por otro lado, el ajuste de los parámetros de implantación mediante el programa de simulación TRIM ha permitido definir un proceso de implantación en cuatro etapas para al formación de una capa continua de SiC de composición estequiométrica. El análisis de las muestras implantadas en este proceso ha permitido corroborar la formación de una capa enterrada y continua de β-SiC con interficies abruptas entre la capa y las regiones superior de Si y del substrato. Estas capas enterradas han sido aplicadas con éxito a la síntesis de simples dispositivos micromecánicos de test. Para ello, es necesario realizar un análisis previo de las propiedades de paro de ataque químico de C implantado en Si. Es interesante determinar la cantidad mínima de C necesario para un comportamiento idóneo de paro. Medidas de SIMS realizadas en muestras atacadas con TMAH (25% wt, 80°C) han permitido determinar este valor de concentración alrededor de $1.7x10^{22}$ ions/cm^2, que corresponde a una dosis mínima de paro de ataque químico en el rango de $2\text{-}3x10^{17}$ cm^{-2} para las condiciones de implantación utilizadas (300 keV a 500°C). Estos datos han sido interpretados usando un modelo de percolación y asumiendo una estructura Si/SiC binaria en la capa enterrada.

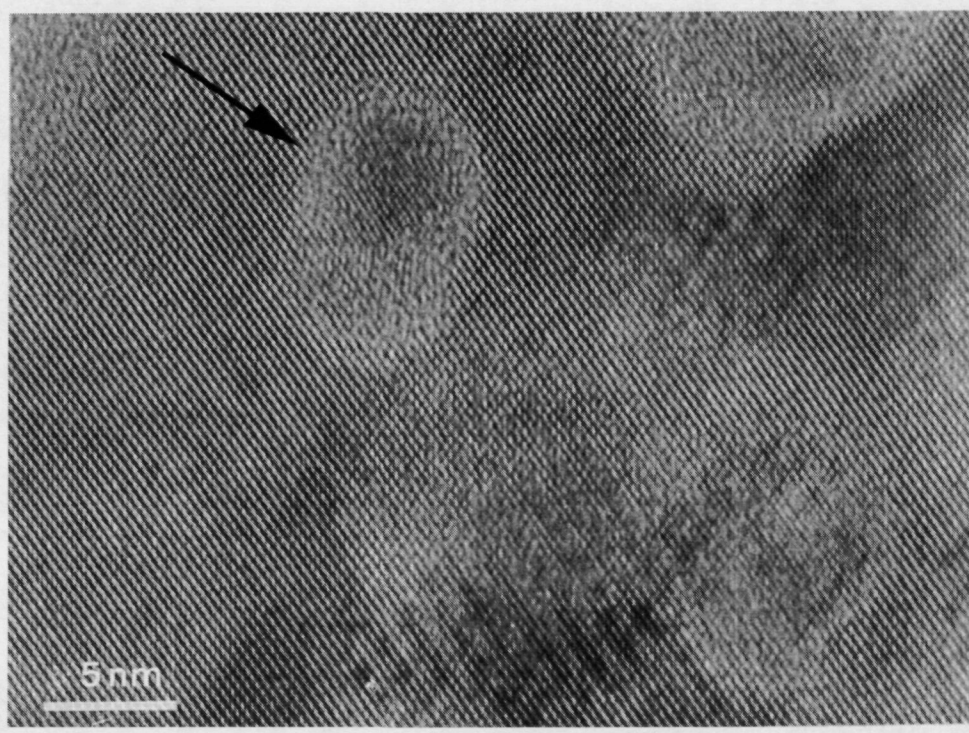

Figura 6 Imagen de TEM de alta resolución de Si implantado con C a 500ºC, mostrando precipitados de β-Si, rodeados de una envoltura de contraste amorfo.

La alta calidad estructural de las capas sintetizadas, que muestran una extrema selectividad de ataque químico en relación con la red de Si, junto a la abrupticidad de todas las interficies Si/SiC y la baja tensión residual después del tratamiento de recocido térmico ha permitido fabricar estructuras de test suspendidas como membranas, puentes y 'cantilevels'. En ese sentido, el alto grado de dureza del SiC permite la fabricación de haces de hasta 100 μm de longitud y 40 μm de anchura, con un grosor mínimo (alrededor de 300 nm). Las capas implantadas pueden también ser usadas como base para el crecimiento de capas mas gruesas de SiC, con ventajas potenciales sobre capas crecidas usando técnicas del tipo CVD sobre substratos de Si.

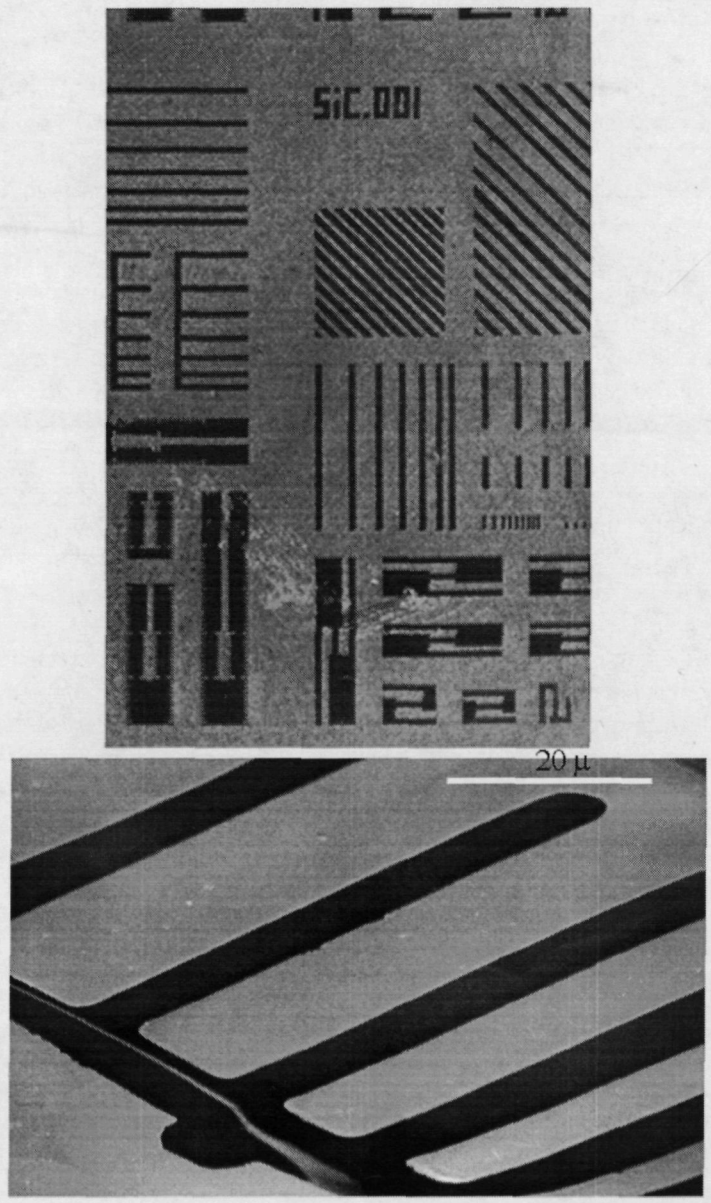

Figura 7 Imagenes SEM de una microestructura obtenida tras la implantación a 500ºC de C en Si, su posterior recocido, y finalmente un ataque químico para eliminar el Si.

7. Implantación de Carbono en aleaciones de SiGe

Se han sintetizado estructuras SiGe/SiC por implantación iónica de C a medias y altas dosis a RT en capas amorfas de $Si_{1-x}Ge_x$. Los datos obtenidos demuestras que tanto la incorporación de C en posiciones sustitucionales en la red como la formación de cristales de SiC vienen determinadas por la concentración de C presente en las muestras. Para concentraciones de hasta el 1-2%, el C se incorpora preferentemente posiciones sustitucionales en la red de Si y no se observa trazas de formación de SiC incluso recociendo térmicamente a 900ºC, a pesar de que a esta temperatura se detecta un decrecimiento del C sustitucional incorporado a la red. Para concentraciones mayores de hasta el 15%, coexisten C en posiciones sustitucionales y SiC cristalino altamente distorsionado. Un incremento en la concentración de C en la región implantada hasta un máximo del orden del 37% conlleva una drástica mejora de la cristalinidad de los granos de SiC, junto con la ausencia de señal relacionada con el C sustitucional.

El crecimiento distorsionado de los precipitados de SiC observado a dosis correspondientes a concentraciones de C intermedias (con concentraciones máximas del 15%) podría estar relacionado con la formación de agregados de Si y C en posición sustitucional, como paso intermedio entre la incorporación del C en posiciones sustitucionales de la red (que tiene lugar fundamentalmente para concentraciones inferiores a 1-2%) y la formación de SiC (que es dominante para concentraciones mayores de C). Por otra parte, los espectros Raman medidos en las capas implantadas sugieren que la incorporación de C en posiciones sustitucionales de la red tiene lugar de forma preferente en la región del substrato de Si que recristaliza de forma epitaxial con el recocido. La ausencia de C sustitucional en los cristales de SiGe podría estar relacionada con la mayor distorsión local de la red de SiGe, con respecto a la de Si, alrededor de los atomos de C en posiciones sustitucionales, como consecuencia del aumento del parámetro de red con el contenido de Ge en la aleación SiGe.

Por otra parte, se han caracterizado procesos de implantación iónica a alta temperatura (500ºC) en capas epitaxiales de $Si_{1-x}Ge_x$ tensionadas (x=0.27) y relajadas (x=0.56). Las condiciones de implantación utilizadas han sido seleccionadas para obtener una concentración máxima de C igual a la de Ge en la capa, x. De acuerdo con los resultados obtenidos anteriormente sobre la implantación de capas amorfas, para estas dosis de implantación no se espera la incorporación de C en posiciones sustitucionales de la red de Si o SiGe dando lugar a aleaciones metaestables binarias o ternarias. Esto concuerda con los resultados experimentales, que muestran la síntesis directa de cristales de β-SiC en la capa implantada, con la misma orientación cristalina que el substrato de Si.

La comparación entre la implantación sobre estas capas epitaxiales de SiGe y otras análogas sobre substrato de Si muestra la existencia de importantes diferencias relacionadas con los parámetros de red y la tensión de la red del substrato previa a la implantación. Para la red relajada de SiGe, existe un incremento en la tensión residual de lo granos de SiC, causada por el mayor volumen que queda libre determinado por la inyección de átomos en posiciones intersticiales, principalmente los de Ge, desde la región implantada. Esta mayor distorsión elástica de los cristales está acompañada por un mayor grado de desorientación en relación con la red de SiGe. Este comportamiento contrasta con el de las capas totalmente tensionadas de SiGe. En este caso, el crecimiento de los cristales de SiC ocurre bajo una tensión biaxial compresiva, lo que lleva a una mejora tanto en la tensión tensil residual como en la orientación cristalina de los cristales de β-SiC en relación con la red de SiGe.

Finalmente, cabe destacar que en todos los casos estudiados (implantación a RT de capas amorfas o implantación a alta temperatura de capas epitaxiales), la formación del SiC viene acompañada de una fuerte migración de los átomos de Ge de la capa implantada. Este fenómeno es debido a la mayor estabilidad del enlace Si-C frente al Ge-C, y conduce a la formación de estructuras multicapa SiGe/SiC complejas. Para las capas epitaxiales tensionadas, el enriquecimiento en Ge de la red de SiGe determina su relajación. Estos resultados muestran la fuerte tendencia de los sistemas implantados hacia la separación en las fases cristalinas β-SiC y SiGe.

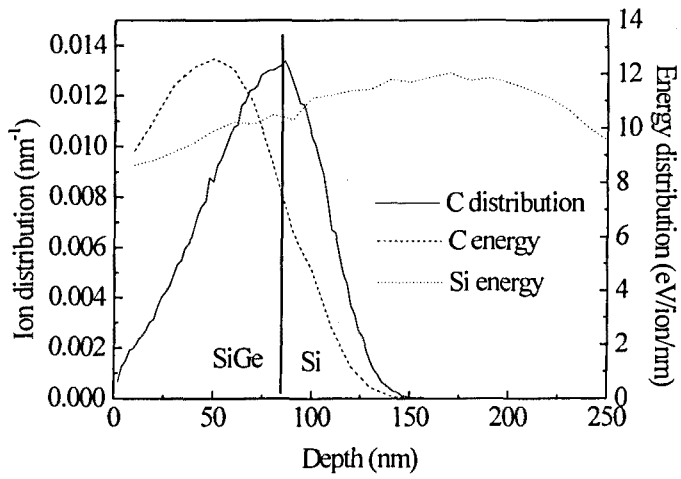

Figura 8 Perfil de implantación de C en SiGe sobre Si simulado por TRIM.

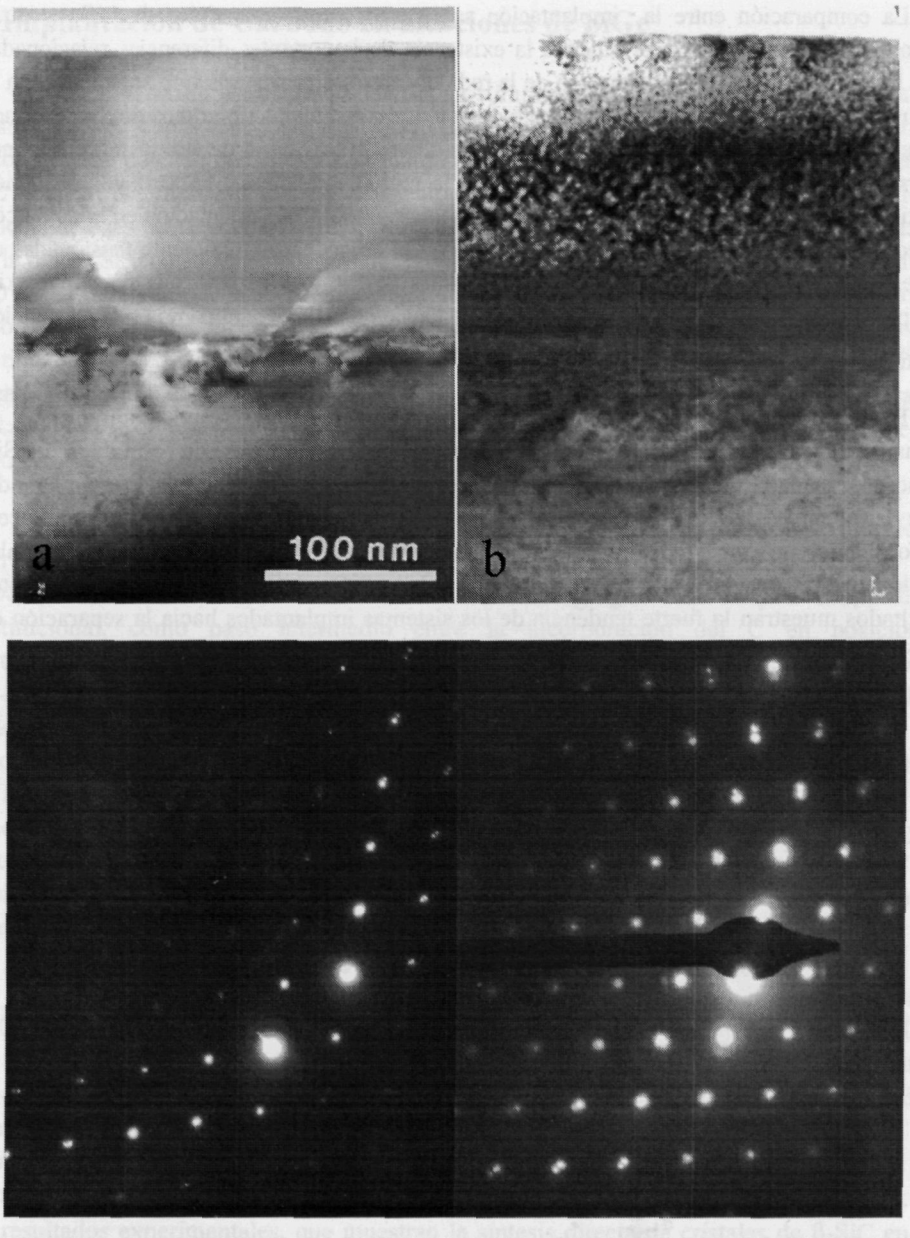

Figura 9 Imagenes TEM y patrones de difracción de SiGe sobre Si antes y después de ser implantado con C.